Multiparameter Flowfield Measurements in High-Pressure, Cryogenic Environments Using Femtosecond Lasers

Ross A. Burns[1] and Paul M. Danehy[2]
NASA Langley Research Center, Hampton, VA, 23681

and

Christopher J. Peters[3]
Princeton University, Princeton, NJ, 08544

Femtosecond laser electronic excitation tagging (FLEET) and Rayleigh scattering (RS) from a femtosecond laser are demonstrated in the NASA Langley 0.3-m Transonic Cryogenic Tunnel (TCT). The measured signals from these techniques are examined for their thermodynamic dependencies in pure nitrogen. The FLEET signal intensity and signal lifetimes are found to scale primarily with the gas density, as does the RS signal. Several models are developed, which capture these physical behaviors. Notably, the FLEET and Rayleigh scattering intensities scale linearly with the flow density, while the FLEET signal decay rates are a more complex function of the thermodynamic state of the gas. The measurement of various flow properties are demonstrated using these techniques. While density was directly measured from the signal intensities and FLEET signal lifetime, temperature and pressure were measured using the simultaneous FLEET velocity measurements while assuming the flow had a constant total enthalpy. Measurements of density, temperature, and pressure from the FLEET signal are made with accuracies as high as 5.3 percent, 0.62 percent, and 6.2 percent, respectively, while precisions were approximately 10 percent, 0.26 percent, and 11 percent for these same quantities. Similar measurements of density from Rayleigh scattering showed an overall accuracy of 3.5 percent and a precision of 10.2 percent over a limited temperature range (T > 195 K). These measurements suggest a high degree of utility at using the femtosecond-laser based diagnostics for making multiparameter measurements in high-pressure, cryogenic environments such as large-scale TCT facilities.

Nomenclature

Symbols

f	=	lens focal distance
h	=	enthalpy [J/kg]
I	=	Intensity
P	=	pressure [kPa]
r	=	radial coordinate
s	=	generic distance
t	=	time [s]
T	=	temperature [K]
u	=	velocity [m/s]
x	=	stream-wise coordinate
y	=	wall-normal coordinate
z	=	span-wise coordinate

Fit Coefficients

A	=	SRGE surface fitting
B	=	RS background subtraction
C	=	FLEET decay rate power-law fitting
D	=	FLEET decay rate empirical fitting

Subscripts and indices

EF	=	empirical fit
$FLEET$	=	FLEET
i	=	directional index
j	=	burst index
n	=	generic position index
PLF	=	power-law fit

[1] Research Engineer, National Institute of Aerospace, AIAA Member.
[2] Research Scientist, Advanced Measurements and Data Systems Branch, AIAA Associate Fellow.
[3] NSTRF Fellow, Department of Mechanical and Aerospace Engineering, AIAA Student Member.

Greek Symbols

ε	=	Standard error/accuracy
γ	=	FLEET signal decay rate
ρ	=	gaseous mass density [kg/m^3]
σ	=	standard deviation
τ	=	FLEET signal lifetime
θ	=	polar coordinate

RS	=	Rayleigh scattering
t	=	total (stagnation) condition
$\|\|u\|\|$	=	constant total enthalpy
0	=	reference condition

I. Introduction

ADVANCING the predictive capabilities of complex flow simulations and assessing the uncertainties surrounding their results relies in part on the availability of high-fidelity experimental data for validation.[1,2] While widely available for small-scale wind tunnels, the experimental data available for large-scale flow facilities, such as those at the various NASA centers, are much harder to find. In particular, there is often a significant lack of information regarding true conditions encountered during testing including knowledge of the freestream velocity, vorticity, composition, and thermodynamic properties, true model and facility shapes, the state of leading edge boundary layers on models, and so forth. As these data often serve as inputs to relevant simulations, achieving convergence between experimental and simulation conditions is rarely assured. Furthermore, measurements of velocities and off-body thermodynamic conditions in these large-scale facilities for validating simulations are similarly uncommon in the literature.

A particularly difficult class of facilities to evaluate at this level of detail are known as transonic cryogenic wind tunnels (TCTs for brevity), which include facilities such as the European Transonic Windtunnel (ETW) and the National Transonic Facility (NTF) at NASA Langley Research Center. While these facilities are prized for their ability to produce flight-accurate Reynolds numbers, the manner in which they operate has heretofore made it difficult to establish the true state of the test section during experiments. Specifically, these facilities (typically) operate by injecting cryogenic liquid nitrogen into the flow path, greatly reducing the operating gas temperature and viscosity while simultaneously increasing the density to increase the Reynolds number.[3,4,5] Since these facilities operate close to the liquid-gaseous saturation point, there is often a significant degree of uncertainty surrounding the composition of the test fluid. Moreover, the injection and mixing struts placed within the flow paths of the facilities can lead to non-uniform distributions of freestream turbulence and vorticity.[6] Finally, due to the very low temperatures experienced within the facilities, contraction of models and test section walls can alter the aerodynamic shape of the flow path during the course of a test. While all of these parameters could, in principle, be measured, constructing the facilities to operate in these extreme conditions often limits the scope of experiments that can be performed in this service. As a result, many customer tests only involve integrated drag, lift, and moment measurements in addition to standard wall-based temperature and pressure measurements.[7]

To quantify the state of the inflow conditions in TCT facilities, physical probes are often needed including hotwire anemometers and pitot rakes for measuring velocities and pressures.[6,8] The reasons for this limitation to physical probes can vary, but often optical diagnostics that utilize molecular or particulate seeding are functionally prohibited. Particle image velocimetry (PIV) and Doppler global velocimetry (DGV) were at one time accomplished in ETW by injecting steam-saturated nitrogen into the flow circuit for seeding.[9,10] Operational protocols still prohibit this and other artificial seeding methodologies at many TCT facilities (including NTF) as there is a high risk of contaminating the flow circuit with residual water or any other seeding medium. Only two successful applications of particle-based velocimetry were demonstrated at the NASA TCT facilities, which used laser Doppler velocimetry[11] and laser transit anemometry,[12] and the naturally-occurring seeding used was present inconsistently and was quite limited in its range of applicable tunnel conditions. Evaluation of off-body thermodynamic conditions poses a different set of challenges to researchers. The measurement of surface pressures and temperatures can be achieved using pressure- and temperature-sensitive paints, respectively, and have been done to modest success in both the European and American TCT facilities.[13,14] However, the optical measurement of off-body temperatures and pressures has not thus far been achieved. Temperature-sensitive particles, which have been designed to function as thermographic PIV tracers, lose sensitivity at the temperature range of interest and are often too large to accurately track flow features in the transonic regime (in addition to being prohibited for being particles).[15] Furthermore, the application of a technique such as coherent anti-Stokes Raman spectroscopy (CARS), which requires very accurate alignment of multiple laser beams, is impractical in TCT facilities due to the high amplitude vibrations and limited optical access.

The present study is part of an ongoing effort to improve the measurement capabilities at NASA Langley Research Center in support of characterizing flow conditions for complex fluid dynamical simulations. This paper documents a series of investigations done in the NASA Langley 0.3-m TCT facility to evaluate commercial femtosecond laser technology for making multi-parameter flowfield measurements in high-pressure, cryogenic environments. Two independent optical effects are concurrently investigated for their potential in this regard. The first of these studies involves a nonlinear optical phenomenon known as femtosecond laser electronic excitation tagging (FLEET).[16] In a previous study, the FLEET effect was shown to serve as an excellent marker for use in time-of-flight velocity measurements in the same facility, possessing both marked accuracy and precision.[17] FLEET has also exhibited some utility in measuring certain thermodynamic properties over limited ranges of conditions. Previously, spectrally resolved FLEET signal was used to make measurements of temperature in a heated jet at atmospheric pressures.[18] Additionally, the FLEET signal has been shown to have significant sensitivity to pressure at standard temperature conditions, though the observed trends did not monotonically increase or decrease in such a way to permit a direct pressure measurement.[19] Rayleigh scattering (RS) from the femtosecond laser pulses is also investigated for its utility as a density measurement. Density measurements based on Rayleigh scattering have been made widely in a range of different flow regimes.[20] The measurement of molecular nitrogen densities has previously been achieved by applying Rayleigh scattering in the NASA Langley 0.3-m TCT.[21,22] In these past tests, there were difficulties in maintaining laser energy stability due to thermal fluctuations and facility vibrations, and independent verification of the results was not possible due to the nature of the fluid dynamics test performed concurrently.

In the present studies, in addition to its use as a velocimetry technique the FLEET signal intensity and lifetime are investigated for their thermodynamic dependencies and use in evaluating flow properties in high-pressure, cryogenic environments. Measurements of Rayleigh scattering signal intensity from the same femtosecond laser pulses used to generate the FLEET signal are investigated for their utility in measuring freestream densities. The thermodynamic dependencies of these three measured quantities are examined in detail. Several empirical models are then constructed, which capture the behavior of the FLEET signal decay rate and signal intensities. Finally, these models are employed to make measurements of the freestream flow conditions, which are then compared to measurements made by the facility data acquisition system (DAS) to assess their accuracy. This paper is structured as follows: after this introduction, the experimental setup is discussed. The various analytical methods used in assessing the data are then reviewed, followed by an in-depth discussion of the test results and major conclusions.

II. Experimental Program

The test facility, optical systems, and data acquisition systems that were used in these tests are herein described.

A. Test Facility

All experiments were conducted in the NASA Langley 0.3-m Transonic Cryogenic Tunnel (0.3-m TCT).[3] This facility is a fan-driven, closed-loop wind tunnel capable of operating with a number of different test gases including air, nitrogen (N_2), and sulfur hexafluoride (SF_6). For these tests, only nitrogen was used, which is required for the highest Reynolds number and lowest temperature operation. The 0.3-m TCT can operate at total pressures ranging from 100 to 400 kPa and total temperatures from 100 to 325 K. Additionally, the facility stably operates at Mach numbers ranging from 0.2 to 0.75, though there is some flexibility on both ends of this range for short durations. A diagram of the facility layout can be found in Fig. 1a.

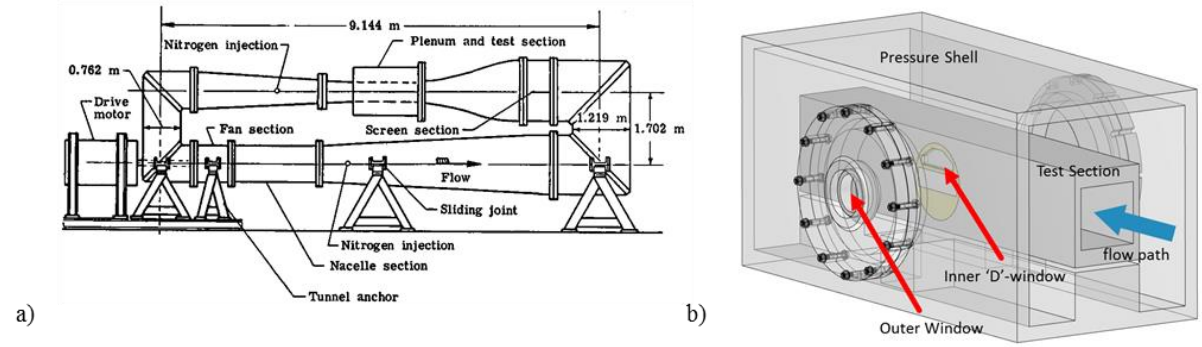

Figure 1. Tunnel layout. a) Overall schematic of 0.3-m TCT facility (from [4]) and b) perspective view of test section and plenum showing optical access.

The 0.3-m TCT test section has a double-shelled construction. The inner test section dimensions are 0.33 m × 0.33 m and is surrounded by an outer plenum of nominally quiescent gas. Optical access for these experiments was afforded by a pair of fused silica windows; one large circular window penetrated the outer plenum, while a smaller 'D'-shaped irregular hexagonal window allowed access to the inner test section. The general test section layout with window locations is shown in Fig. 1b.

B. Laser and Optical Systems

The FLEET measurements utilized a pulsed, regeneratively-amplified Ti:sapphire laser (Spectra-Physics Solstice) with a center wavelength of 800 nm, bandwidth of 20 nm, and a repetition rate of 1 kHz. Data sets were collected with pulse energies around 1.2 mJ, although between 30 to 50 percent of this energy was attenuated through the beam path. The laser system was situated on a platform roughly 3 m above the test section; the beam was brought down to the level of the facility with a pair of periscopic mirrors.

When running at ambient and elevated temperatures the beam was passed straight through the outer window of the plenum before going through a f = +250-mm spherical lens and the inner 'D'-shaped window. If operating the tunnel at cryogenic conditions, after passing through the outer plenum window, the beam was routed through an internal periscope, which was situated inside an evacuated pressure vessel (herein referred to as the *laser conduit*). Due to the large temperature gradient between the plenum and the surrounding environment, large density fluctuations are known to exist within the facility plenum.[4,5] At the time of the test, it was believed that these density fluctuations were responsible for beam-steering and wavefront distortion in the femtosecond laser pulses, which inhibited proper beam focusing and a loss of signal below 200 K in a previous test.[17] The evacuated periscope, functioning similarly to a solution proposed in Ref. 5, was designed to limit the exposure the beam had to this optically unfavorable environment. Figure 2 shows an image of the laser conduit within the plenum. Following this periscope, the beam passed through a f = +200-mm spherical lens before entering the test section through the 'D'-window. In both optical setups, the fs laser pulse came to a focus roughly half-way through the test section, 55 mm from the top wall. Rayleigh scattering originating from this same laser pulse was also detected, as described in the next section.

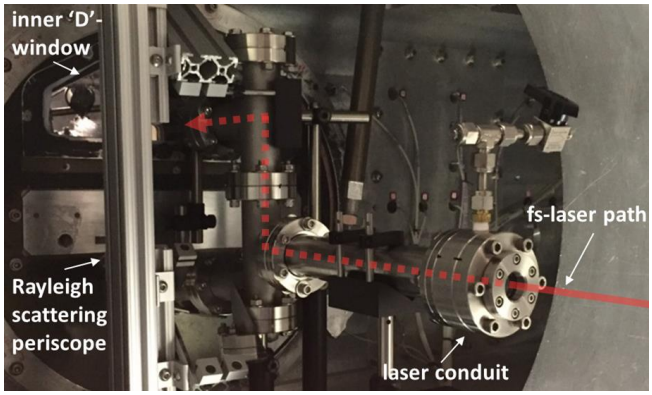

Figure 2. Image of laser conduit and RS periscope within 0.3-m TCT plenum.

C. Data Acquisition Systems

1. Imaging Systems

The FLEET signal was captured with a high-speed image intensifier (LaVision HS-IRO) lens-coupled high-speed CMOS camera (Photron SA-X2). Imaging was done through a 135-mm, f/2 lens and a shortpass optical filter that transmitted wavelengths between 320 and 775 nm. The FLEET camera system was operated in a triggered burst mode; bursts of 15 images were captured at 200 kHz with 100 such bursts being captured per second. A lower burst acquisition rate was used in comparison to the previous tests[17] (100 Hz vs. 1000 Hz) to ensure several full tunnel transit times (roughly 4 seconds at the lowest flow rates) had occurred during the data collection. This change allowed for both the identification of long term trends in the velocity and potentially prevented biasing in the measured velocities and fluctuations. The first image with FLEET signal occurred approximately 70 ns after the laser pulse, while the preceding images were used for background subtraction in post-processing. The FLEET camera system was situated perpendicular to the test section and imaged through both the outer plenum window and internal window to view the FLEET signal in a quasi-boresight configuration, where the camera view is nearly parallel to the direction of laser propagation.

Rayleigh scattering imaging used a high-sensitivity scientific CMOS camera (LaVision Imager sCMOS) equipped with a 105-mm, $f/2$ lens and bandpass filter (centered at 800 nm, with a 25 nm FWHM bandwidth), used to pass the Rayleigh scattering while rejecting the FLEET signal. The optical filter was required because the camera, which is unintensified, had exposure times that would have collected the FLEET emission in addition to the desired scattering signal. Imaging was usually done at 100 Hz, with a 4 ms exposure time; scatter from 4 successive laser pulses was captured in each image to increase the signal intensity above the noise floor of the images. A limited number of single-shot images were also obtained at some of the highest density conditions tested. To perform the Rayleigh imaging concurrently with the FLEET measurements, a mirror and periscope system routed the camera line-of-sight to be, first, orthogonal to the test section, and subsequently, up and through the inner 'D'-window. An image of the internal periscope components can be seen in Fig. 2, while the relative positions of the two cameras and their optical paths can be seen schematically in Fig. 3.

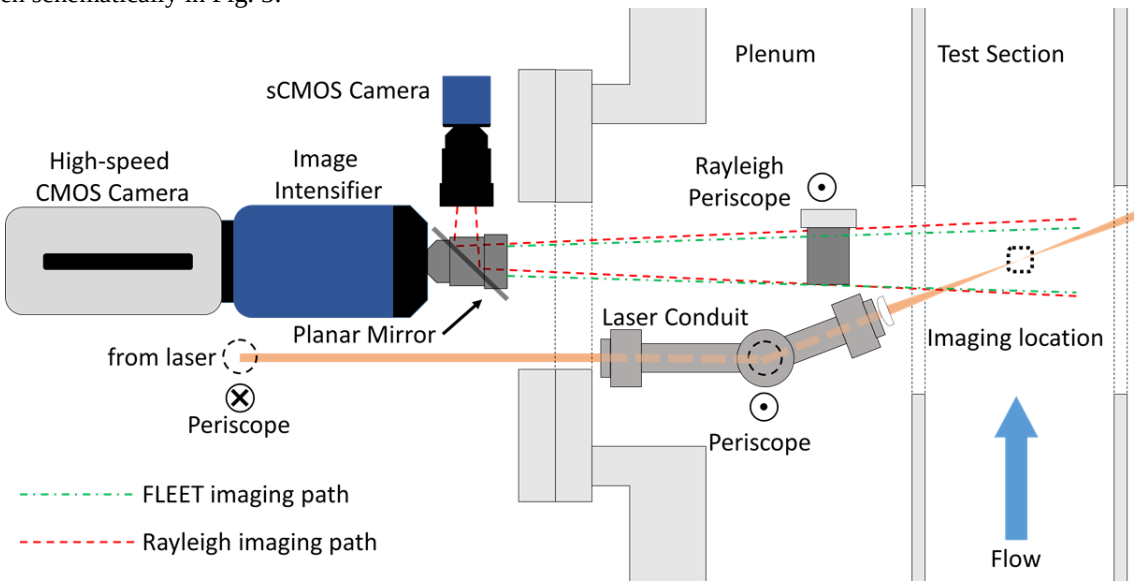

Figure 3. Diagram (top-view) of overall optical setup.

2. Facility DAS

In addition to the camera system, an extensive facility data acquisition system measured the relevant conditions in the tunnel. This system comprised an array of static and total pressure probes throughout the facility, as well as thermocouple probes and strain gauges. These data were read into a network of facility computer systems for processing. Velocities were calculated based on static and total pressure probes and a total temperature probe in conjunction with a real-gas equation of state (EOS, Beattie-Bridgeman equation[23]) for computing the density of the gas. For each FLEET data run (lasting approximately 10 s or 10,000 laser pulses), a data point from the facility system was collected for use in validation and verification of the velocity and thermodynamic data in post-processing.

III. Data Analysis

The following section describes the methods, which were used in evaluating the various types of data collected in these experiments. These analytical methods cover the processing of raw FLEET signal data, the evaluation of velocities, extraction of FLEET signal lifetimes, and the overall processing of Rayleigh scattering data.

A. FLEET Signal Processing

A sample of the raw FLEET data is shown in Fig. 4a. Unlike the previous test, which showed a nearly axisymmetric intensity distribution, the FLEET data are much more ragged in appearance and lack radial symmetry. Consequently, the processing algorithms used previously needed to be generalized to accommodate the new data. Processing of the raw fleet data required many steps to achieve a usable form. The images first underwent a dark-field correction to prevent interference from any mean background intensity. The next steps transformed the background-subtracted FLEET images into analytic functions so that both position and intensity information could be ascertained with high precision and accuracy. The processing kernel consisted of two parts: a location step and a surface-fitting step. The location step was used to mark the rough location of the centroid in the data, which became necessary when the signal intensities were lower. For the first image in a burst, the initial centroid location was assumed to be the point of highest

intensity in the image; this was generally a valid assumption. Were this assumption to become invalid, the data was of too low a signal-to-noise ratio (SNR) to use effectively. For all subsequent images, two-dimensional cross-correlation was performed twice: once between the first image and the n^{th} image and once between the $n-1^{\text{st}}$ image and the n^{th} image. This step allowed for the determination of the centroid of the FLEET signal to be discerned within approximately half a pixel, and further provided a self-contained check to ensure that noise wasn't biasing the result. The displacements obtained in this way were then used to mark out the predicted center of the FLEET signal in the n^{th} image of a burst. Since fine-tuning of this position was to be done later, no sub-pixel interpolation scheme was used in this predictive step.

The next step in the processing kernel was the surface-fitting step; a radially asymmetric, but self-similar intensity profile was fit to the actual FLEET signal intensity. This procedure is initiated by first assuming the position of the peak signal intensity, (x_0, y_0), which is taken from the location step previously described. Next, the coordinate system is transformed to cylindrical (rather than Cartesian) coordinates. In this new coordinate system, a generic ellipsoid (GE) is defined by the equation:

$$r_{GE} = A_1((A_2\cos(\theta-\theta_0))^2 + (A_3\sin(\theta-\theta_0))^2)^{A_4} \quad (1)$$

This function given by Eq. 1 produces an ellipsoid tilted at some angle θ_0, centered at (0,0) in the new coordinate system; the various A_n coefficients refer to parameters which are later fit to the data. The ellipsoid is then shifted and pivoted about the center of the coordinate system by an amount (r_s,θ_s). The distance between the original origin and the perimeter of this now tilted, shifted, and rotated ellipsoid is measured (**s**hifted, **r**otated, **g**eneric **e**llipsoid, $SRGE$).

$$r_{SRGE} = \sqrt{(r_{GE}\cos\theta + r_s\cos\theta_s)^2 + (r_{GE}\sin\theta + r_s\sin\theta_s)^2} \quad (2)$$

The distance prescribed by r_{SRGE} (Eq. 2) is a function solely of the original θ in the transformed coordinate system. This distance is now used as the standard deviation would be in a normal distribution, with the outward distance prescribed by the distance from the location of peak intensity:

$$I(\theta) = I_0\exp\left(-\frac{r(\theta)^2}{r_{SRGE}(\theta)^2}\right) + A_5 \quad (3)$$

Thus the entire intensity distribution is a function of the distance and angle from the location of peak intensity. This function that has been defined possesses an intensity distribution that is self-similar in the polar direction, but is not radially symmetric. A nonlinear least-squares fitting algorithm is used to tune all of the various parameters required for this fit. For some data, a summation of two such spots was necessary to recreate the shape of the original signal as precisely as possible. The original FLEET data is compared to two cross-sectional profiles in Figs. 4b and 4c. As final note to this discussion of the processing kernel, data which saturated the image sensor during acquisition was handled differently. Once the incident signal has saturated the image sensor, there is no further sensitivity to further irradiation. To avoid the potential bias this could impart to the intensity measurements, all pixels with intensities within 0.5 percent of saturation (4075 counts or above in the raw images) were omitted prior to the fitting procedure. Since the gain of the intensifier was adjusted to maximize the dynamic range of the measurement and avoid saturation, the appearance of saturated data was infrequent and typically only occupied one or two pixels within the image of the FLEET signal when it did occur. For further information regarding the linearity of the camera sensor, see Appendix A.

After this processing kernel has been run, the coefficients defining the surface are used to map the analytic function onto a very fine uniform mesh, typically with a spacing of 0.0001 px. This function is then interrogated for four items of information: peak intensity, integrated intensity, location of peak intensity, and location of centroid. Thus, each

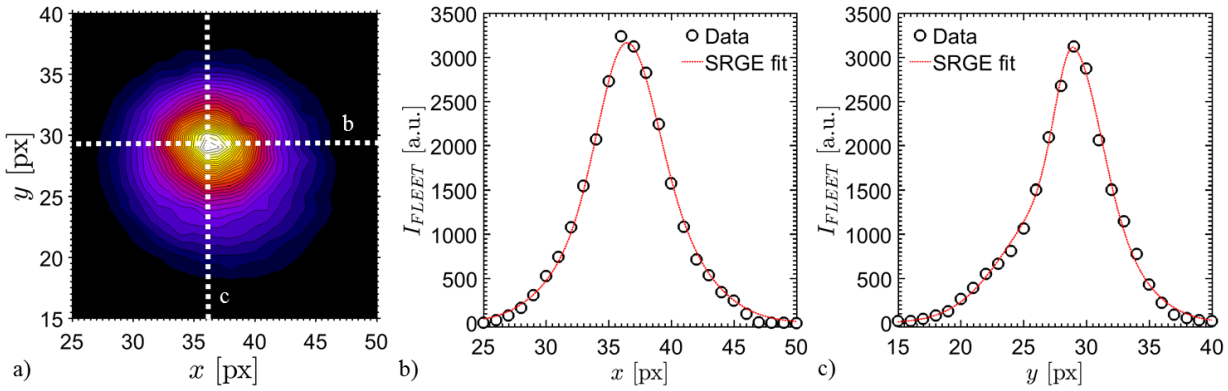

Figure 4. Centerline cross-sectional profiles showing details of SRGE fit. a) Raw data, b) horizontal cross-section, and c) vertical cross-section.

image is ultimately reduced to a small number of values for use in later analysis. The two positions extracted from these data are then transformed to physical coordinates through a nonlinear matrix transform computed from recorded dotcard images.

B. FLEET Velocimetry

Flow velocities were computed for individual bursts by numerically approximating the $x-$ and $y-$ displacements of the FLEET spot with a simple linear fit. Previous efforts used various methods for measuring flow velocities from similar data, including two time-of-flight methods and a polynomial fitting method.[17] While the polynomial fitting method provided an accurate fit to the position data, the measured accelerations were found not to be statistically significant in the present data, since the data was acquired in the freestream where acceleration is low. Thus, a first-order polynomial was fit to the function $s_{i,j}(t)$, where the index i refers to the directional index (x or y), and j refers to the present burst. The measured velocity, $ds_{i,j}/dt$, was then taken to be the slope of this line. A small fraction of data was rejected prior to computing velocities. Notably, FLEET data that exhibited an insufficient fit quality after the processing kernel ($R^2 < 0.7$) or insufficient SNR (SNR < 5) were removed. When this occurred, all samples following the low-quality image in that particular burst were excluded. To ensure an unbiased and sufficient sampling for statistics, only samples computed using the same number of valid frames were used in computing statistics (e.g., if a particular sample was constructed using 11 images and another with only three, the one with three would not be included in the statistics of the 11-frame sets. Instead, the 11-image sets were down-sampled to three images and compared in that fashion), and a threshold of at least 500 samples was required to consider a velocity with a given number of frames.

A sample of the stream-wise velocity measurement statistics from a Mach 0.75 run set are shown in Fig. 5. Figure 5a shows the measured velocity as a function of delay time considered in the fit with the measured 1σ velocity fluctuations plotted as error bars, while three representative velocity probability density functions (PDFs) are depicted in Fig. 5b. A characteristic of this method of evaluating velocities is that, as more frames from the individual bursts are included, the measured standard deviations of the entire dataset rapidly asymptote (much more rapidly than the methods in Ref. 17) to a nearly fixed value, in this case approximately 0.6 percent of the freestream velocity or 1.5 m/s. For each dataset, the ensemble of measured velocities, the mean corresponding to the lowest measured standard deviation of velocity, as well as the standard deviation itself, were stored for later analysis and use in analyzing thermodynamic conditions.

In the present studies, the lower limit on the velocity precision was measured to be 0.4 m/s (measured in quiescent N_2), which represents a nearly 20 percent decrease (i.e.,improvement) over the measurements taken in the previous test.[17] Moreover, there was an overall improvement to the quality of the data: more frames and bursts contained usable data, and the dependence of the FLEET signal lifetime on the Mach number was no longer present (since attributed to an occluded laser beam and the motion of the tunnel in response to changing operating conditions). Ultimately, these improvements allowed for larger data ensembles as well as an improved sensitivity to freestream velocity fluctuations; consistent statistics could be generated with larger numbers of frames independent of the operating conditions. Since this paper is focused on the thermodynamic behavior of the signals and their use in evaluating the tunnel conditions,

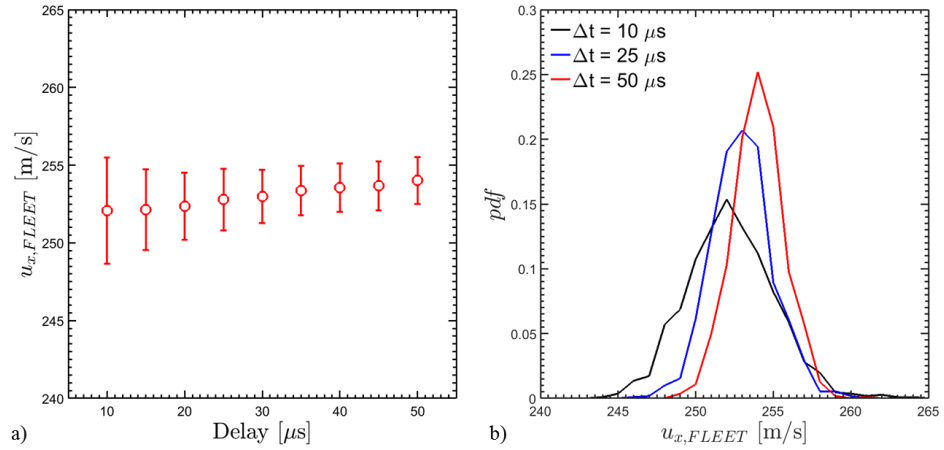

Figure 5. Sample velocity measurement from a Mach 0.75 data run. a) Evolution of mean velocity with an increasing number of frames and b) sample velocity pdfs at different time delays.

any further discussion of the velocity will be omitted in the results. The measurement accuracy for the velocity was found to be approximately within 1.5 percent, while the measured velocity fluctuations ranged from 0.3 percent to 5.6 percent, with the mean level of fluctuations lying at 0.7 percent.

C. FLEET Signal Lifetime

Using the procedure outlined in Section III.A, extensive time series of FLEET signal intensities could be constructed. One such trace is depicted in Fig. 6, collected with a sampling rate of 400 kHz. As will be shown in subsequent sections, the decay of the FLEET signal intensity is strongly tied to the thermodynamic properties of the surrounding gas. Thus, there was interest in studying the variations of the signal lifetime with respect to said conditions. However, during the course of the analysis, it was found that representing the decay with exponentials was quite cumbersome. The decay curves in Fig. 6a and b are fit with representative exponential functions to show the resulting quality of the fit. The true signal decay is best modeled with a tri-exponential function; this function is the only way to capture the long-term behavior of the signal intensity. However, the large number of correlations that could be constructed and analyzed for dependence in this manner, including the individual lifetimes, ratios of lifetimes, ratio of each component of the exponential to the entire decay curve, and so forth, made it difficult to get a clear picture of the thermodynamic behavior. To simplify the analysis, an empirical approach was taken to model the lifetimes. Each signal decay curve was first fit was a tri-exponential function to capture its total decay behavior. From this analytical fit, two different values were extracted: the time it took the signal to fall to $1/e$ of its initial value (henceforth called τ_1), and the time it took to fall to $1/e^2$ of its original value (τ_2). These two 'lifetimes' were then used in all the analysis that follows. While this approach was originally taken to avoid the complexities of modeling the sheer number of parameters involved in the fitting procedure, it also proved to be more resistant to experimental noise than the direct fitting method since it was not functionally dependent on the exact values of the fitting parameters.

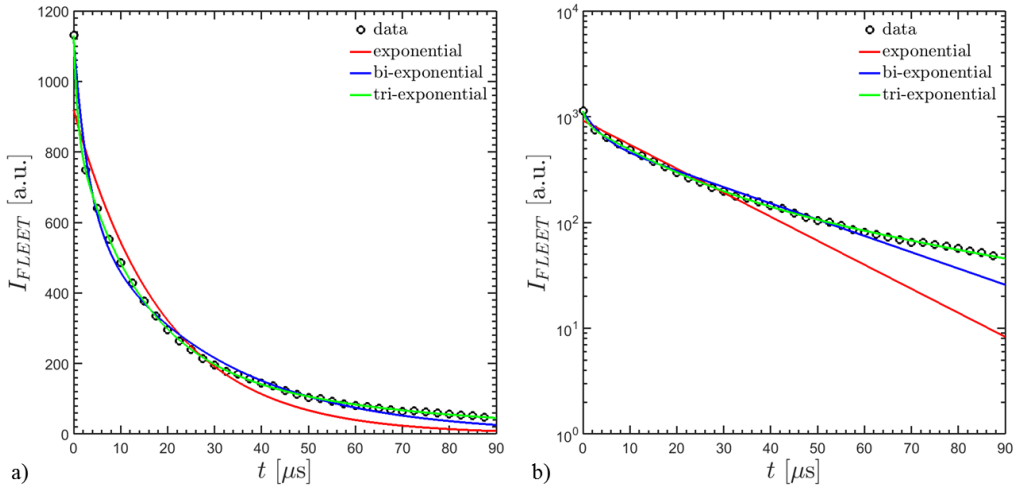

Figure 6. Example FLEET signal decay curve and exponential fits to data. a) Linear intensity scale and b) logarithmic intensity scale.

D. Rayleigh Scattering

A sample raw Rayleigh scattering image (containing some FLEET signal at the focus) is shown in Fig. 7a. The processing of these data involved, first, the rotation of the image to align the Rayleigh scattering signal with the image coordinates. After rotation, the images were cropped to include only the laser signal and a minimal number of surrounding pixels. Next, a numerical background subtraction procedure was implemented, which fit a bi-directional polynomial to the cropped and rotated raw images, avoiding areas containing the scattering signature. This polynomial was of the form:

$$BG_{RS}(y,z) = B_1(B_2z^2 + B_3z + B_4)(B_5y^2 + B_6y + B_7) + B_8 \quad (4)$$

This background was then subtracted from the raw images. A linear scaling factor is then applied to the image coordinates to bring them into the physical domain. An example of a processed Rayleigh scattering image is shown in Fig. 7b. The columns of each such image were then summed to create a span-wise trace of the RS signal, an example of which is given by Fig. 8.

Evaluation of the Rayleigh scattering signal also required discriminating the Rayleigh scattering from the residual FLEET signal emission present at the center of each image (even though a spectral filter blocked most of the FLEET signal). To do this, the Rayleigh scattering signal was assumed to be the mean signal of the first 50 data points on both sides of the signal trace. The sample trace shown in Fig. 8 has these regions highlighted in red. These data were taken for every Rayleigh scattering image collected, and the ensemble, mean, and standard deviations were kept for use in later analysis.

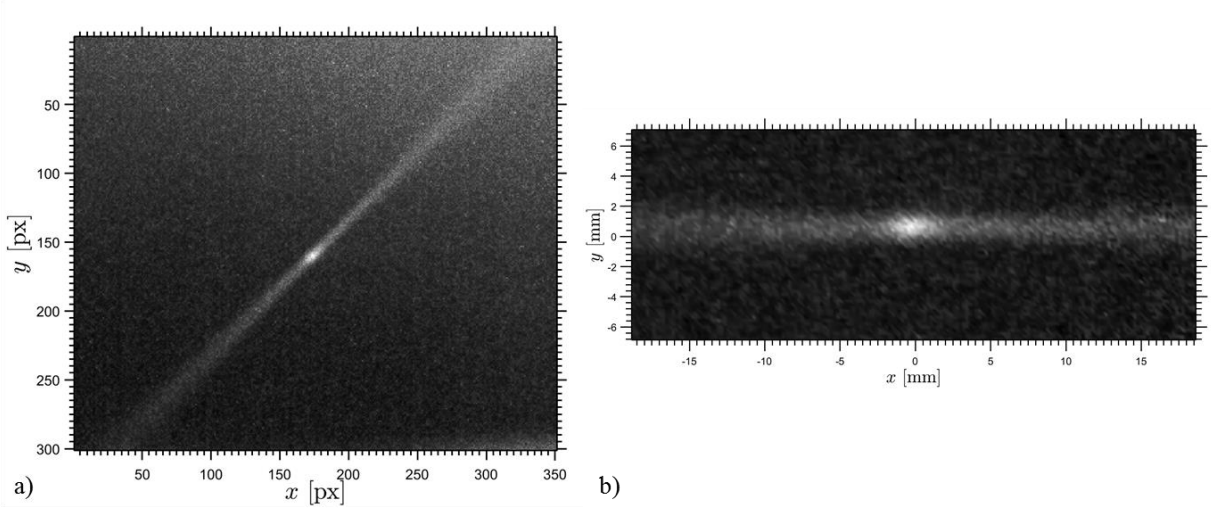

Figure 7. Sample Rayleigh scattering images. a) Raw RS image and b) processed RS image.

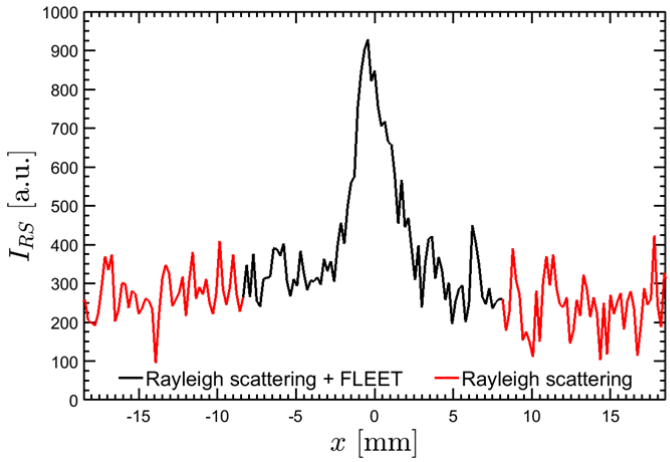

Figure 8. Sample Rayleigh scattering signal trace. Pure RS signal is highlighted.

IV. Results and Discussion

The results from these tests are broken into three primary sections: the thermodynamic dependencies of the FLEET and Rayleigh scattering signals, modeling the behavior of these signals, and the estimation of thermodynamic conditions within the facility.

A. Thermodynamic Dependencies of FLEET and Rayleigh scattering signals

1. FLEET signal intensity

The response of the FLEET signal to reduced pressure in air and molecular nitrogen has been studied in some detail by DeLuca et al.[19] These studies, which were conducted at standard temperatures, did not exhibit a monotonic

trend with respect to the pressure. Rather, the signal was found to follow two distinct behavioral trends, depending on the pressure regime. At the higher end of their pressure domain (approximately 100 kPa), the FLEET signal intensity was found to be proportional to pressure. At intermediate pressures (1-10 kPa), the gas behaved very differently depending on its composition. In air, the signal leveled off and was found to be largely insensitive to pressure. In N_2, the signal began to increase slightly as pressured decreased in this regime. Finally at still lower pressures, the signal rapidly climbed and leveled off in air, while in nitrogen, the FLEET signal slowly decreased as the pressure was reduced. Given the complex kinetics involved in the generation and sustenance of the FLEET signal, attempting to extrapolate these trends to the high-pressure, high-density regimes present in TCT-type facilities is likely to yield inconsistent results at best. Thus, there is merit in studying the fundamental response of the FLEET signal intensity in the desired regime.

The initial FLEET signal intensity measured in this testing campaign is plotted as functions of pressure, temperature, and density in Fig. 9. These data were collected 70 to 80 ns after the laser pulse had occurred, and approximately 2000 such shots were used in computing the statistics for each point. These data comprise a rather sizeable matrix of different temperatures and densities, and thus the data that is displayed appears very scattered. In Fig. 9a, it is seen that there is a clear trend of increasing signal intensity with increasing pressure. There is still notable vertical spread of the points at every pressure, suggesting a secondary effect leading to the increase in signal. In fact, the primary difference in these points is the temperature at which they were taken. Notably the highest points at each pressure represent the lowest temperature at that pressure condition. This trend is echoed in Fig. 9b, which shows the same data plotted with respect to temperature. Here again, there is a slight upward trend with decreasing temperature, with the points of highest intensity corresponding to the highest pressure cases. This direct proportionality to pressure and inverse proportionality to temperature suggests that the changes in intensity are largely a density effect. To verify the magnitude of this correlation, Fig. 9c again plots this data with respect to the local static density of the gas. Here a distinct trend becomes apparent; the signal intensity appears to be linearly dependent on the density of the gas. This trend is verified up to approximately 400 kPa pressure and static temperatures as low as 145 K. The observed behavior of the FLEET signal with respect to density over a wide range of temperatures and pressures does suggest some utility in using the FLEET signal intensity as a metric for density in this pressure and temperature regime. The agency of this potential measurement technique is explored in the next two sections.

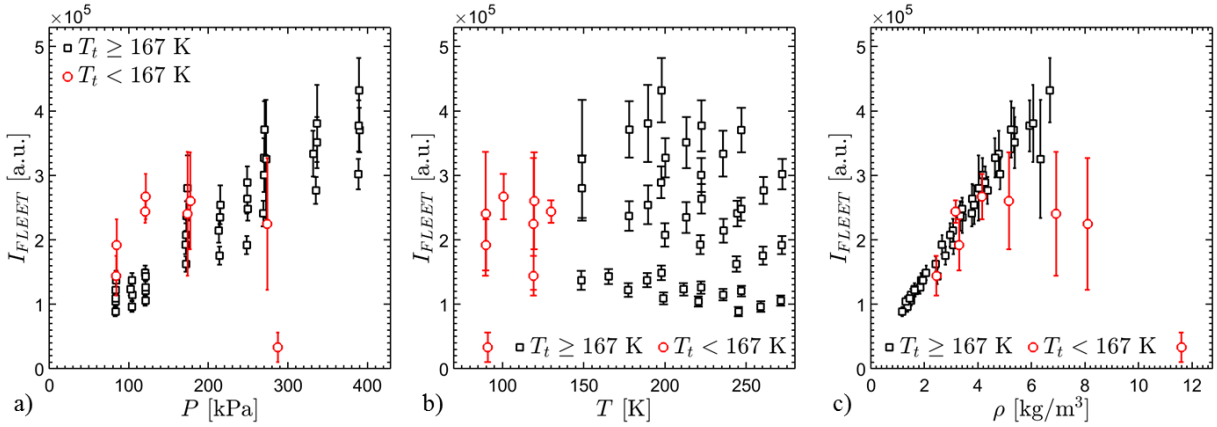

Figure 9. Thermodynamic dependencies of initial FLEET signal intensities. a) Pressure dependence, b) temperature dependence, and c) density dependence.

A final note about these data concerns the range of temperatures over which the data was collected. In Fig. 9, there are a number of points marked in red, which represent data collected below total temperatures of 167 K. This demarcation is made to note a procedural change in the data collection. Specifically, when operating the 0.3-m TCT facility in cryogenic mode, the tunnel slowly contracts as the body of the tunnel cools. As this occurs, the femtosecond laser beam slowly moved out of alignment. Above total temperatures of 167 K, access to the facility was still possible, and so adjustments were made to the optical path to compensate for this contraction. However, on this particular day of testing, a nitrogen leak developed in the vicinity of the tunnel, and direct access to the optics was not possible below this temperature since the leak rate tended to increase as the tunnel experienced further contraction. Consequently, the beam grew increasingly clipped on the laser conduit as the temperature decreased below this point, and the subsequent trend with density fell away. However, it is unclear if the trend would have continued as expected. The points furthest from the linear trend all represent the highest pressure conditions at their respective total temperatures. Thus, it is

possible that a secondary effect is also influencing the measured signal intensities. The nature of this effect is unknown; it is possible the tunnel experiences slight motion as the pressure is changed, exacerbating problems caused by the clipped beam profile. It is also possible that the density fluctuations in the plenum reach a critical level where they begin to alter the beam profile sufficiently to interfere with the FLEET signal generation, even with the presence of the laser conduit. Finally, there could be a transition in the underlying kinetics at high pressures that results in the decreasing intensity. The current data are insufficient to make a clear assertion, but in light of the circumstances, the range of validity for these measurements is to total temperatures above 167 K until further investigation is possible.

2. FLEET signal lifetimes

The thermodynamic dependence of the FLEET signal lifetimes are not well understood; there have been no definitive studies about the behavior of the FLEET signal lifetime and only a few cursory studies. The results from DeLuca et al.[19] have some information regarding the time-evolution of the FLEET signal at reduced pressures. The lifetime of the FLEET signal appears to follow similar trends to the initial signal intensity; a rapid decay is found above 10 kPa or so, while the behavior becomes far more erratic at reduced pressures. Another study by Michael et al.[24] looked at a single case of signal decay (at STP conditions), which indicated a bi-exponential decay over a time history of 10 μs. Thus, there is not a plethora of information regarding the behavior of the FLEET signal lifetime with respect to thermodynamic conditions, with no data currently available for the thermodynamic ranges of interest (80 K to 300 K, 100 to 400 kPa).

As discussed in Section III.C, the signal decays were reduced to two empirical lifetimes to simplify the data analysis. The behaviors of these two lifetimes are plotted against temperature at three different pressures in Fig. 10a-c. Before discussing specific trends, it is worth noting that data on lifetimes was collected with static temperatures as low as 80 K. Despite the misalignment and occlusion of the beam as discussed in Section IV.A.1, the lifetime data was not clearly influenced by this effect. Since the lifetimes are measured relative to the initial signal intensity, the data is self-normalizing, and thus the observed trends were not affected in a similar manner. There is some chance that the reduced energy of the laser pulse is influencing the lifetime of the signal, but there was no clear evidence of such disparity in the data. Looking at the data for the signal decay, clear trends are apparent in both lifetimes. Specifically, both lifetimes decrease with increasing pressure and decreasing temperature, suggestive again of a strong density dependence. This type of trend is also reminiscent of the collisional-quenching of fluorescence, which exhibits similar dependence on the thermodynamic conditions.

To help expound on these observations, the combined lifetime data is plotted as a function of density in Fig. 11. Here again, as with the initial signal intensity, the scatter observed over different thermodynamic conditions collapse into a single trend when plotted against the density. Notably, there is a clear trend of decreasing lifetime with increasing density, though the dependence is not linear as was the case with the initial signal intensity. The observed density dependence suggests further that the signal lifetime or lifetimes could be collectively used as a means to measure density without the limitation imposed on the initial signal intensity by the beam occlusion. Repeated measurements on subsequent testing days, during which adjustments were made to improve the alignment and higher data collection rate was used, confirm the values of the lifetime figures herein presented. The repeatability also indicates that the measured lifetime values, while certainly dependent on the particular optical setup, remain consistent if no major system parameters (lens focal lengths or laser pulse energy) are altered and beam alignment is maintained

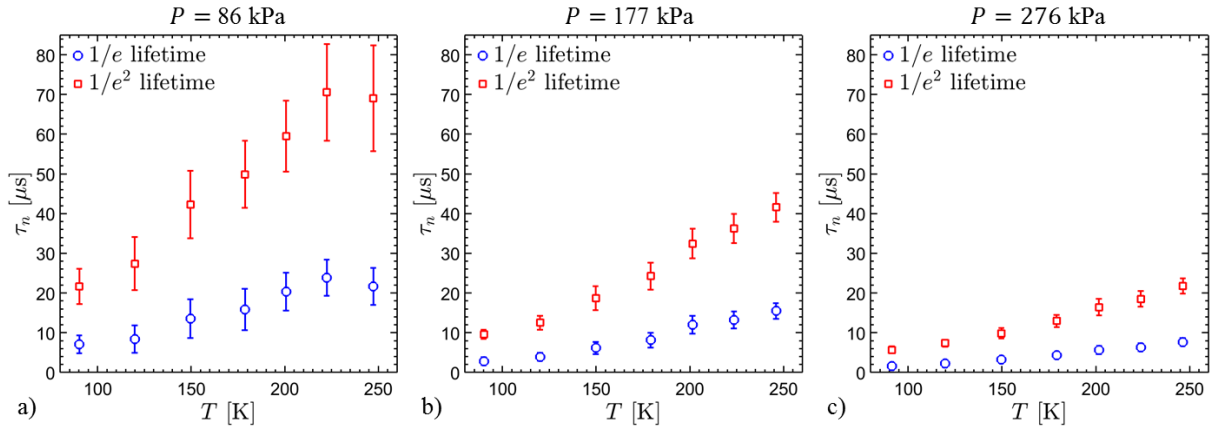

Figure 10. FLEET signal lifetimes versus temperature at different static pressures. a) 86 kPa, b) 177 kPa, and c) 276 kPa.

3. .Rayleigh scattering signal intensity

Rayleigh scattering has been applied on two separate occasions in the NASA Langley 0.3-m TCT facility.[21,22] These experiments, conducted first along a line, and later, with planar measurements, were able to demonstrate Rayleigh scattering signals directly proportional to nitrogen molecular densities over the full range of tunnel operating conditions. However, because of the laser wavelength and low laser energies used in the present experiment, it was unclear whether the scattering efficiency would be sufficiently high to render the Rayleigh scattering measurements viable. The previous measurements were all conducted with Nd:YAG lasers operating at a wavelength of 532 nm, while the femtosecond laser used in these experiments had a center wavelength of 800 nm and a bandwidth of 20 nm. These differences reduce the scattering efficiency by over 80 percent while simultaneously increasing the difficulty of filtering background radiation due to the broader spectrum of the laser pulse. The laser pulse energy also was limited to approximately 1 mJ for the FLEET measurements, reducing the available intensity for single-shot RS imaging.

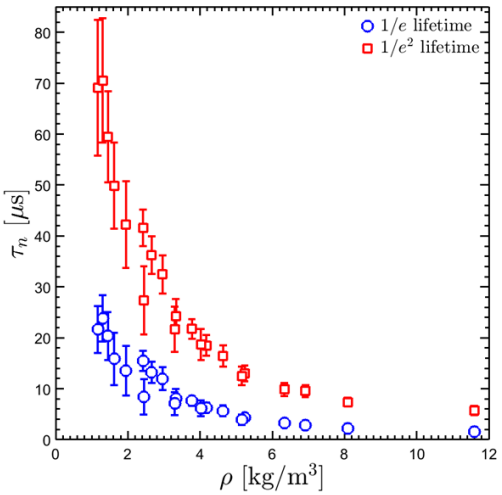

Figure 11. FLEET signal lifetimes versus density.

The measured Rayleigh scattering signal intensity is plotted as a function of gas density over two different total temperature ranges in Fig. 12. For total temperatures greater than or equal to 215 K (Fig. 12a), the signal follows the expected linear trend, indicating a strong correlation between the observed signal and the molecular density of the gas. These measurements were based on the averages of several hundred long-exposure (4 ms) images, each of which captured four laser pulses. While some single-shot images were captured, the observed signals were generally too low to distinguish the scattering from the background intensity except at the highest flow densities. As indicated by Fig. 9, noise within a given image amounted to a RMS noise level of just over 100 counts. With a detection signal-to-noise (SNR) threshold of unity, this made single-shot Rayleigh scattering over the entire range of densities infeasible, and so the results are not herein presented. Nonetheless, the data based on the summed images collected in this study show promise at acting as a density measurement technique within the 0.3-m TCT facility, despite the non-optimal laser used in the measurement. It also should be noted that a change in the optical system such as a camera lens with a higher collection efficiency or an imaging sensor with higher sensitivity or gain could make single-shot RS measurements possible in future tests.

The demarcation at 215 K noted above does not coincide with the misalignment issue experienced with the FLEET signal intensity discussed in Section IV.A.1. At all total temperatures below 215 K, a phenomenon acted to dramatically *increase* the Rayleigh scattering signal. This observation is demonstrated in Fig. 12b. The misalignment of the beam was also observed and intermittently corrected when possible. Since the molecular scattering scales linearly with the incident laser energy, beam misalignment and clipping on the laser conduit would act to decrease the observed intensity. The phenomenon also appeared to happen very inconsistently; there was no obvious trend with pressure or temperature.

In character, the scattering appeared quite different once this problem started occurring. Figure 13 shows three representative scattering images taken at different total temperatures but the same static density (3.35 kg/m^3). The scattering observed in Fig. 13a is characteristic of the scattering seen above 215 K total temperature; faint, uniform scattering is present on the edges of the images flanking a central bright region where the FLEET signal is being generated. The next two conditions, Fig. 13b taken at a total temperature of 133 K and Fig. 13c at 100 K, show two different extents of the scattering phenomenon. To different degrees, the scattering signal has increased by almost an order of magnitude while the central FLEET signal is misshapen. Additionally, Mie scattering from discrete particles was observed in many images, though they are lost in the means shown in Fig. 13.

While only speculation, this dramatic change in the signal character is most likely scattering off of a condensation fog or a byproduct of the liquid nitrogen injection. The size of the individual droplets are, in general, far below the resolution of the camera system but much larger in scattering cross-section than nitrogen molecules. While further work is underway to understand this scattering, it does appear from the time history of these data that the phenomenon is associated with rapid changes in the thermodynamic conditions, notably changes in the pressure. No occurrences of

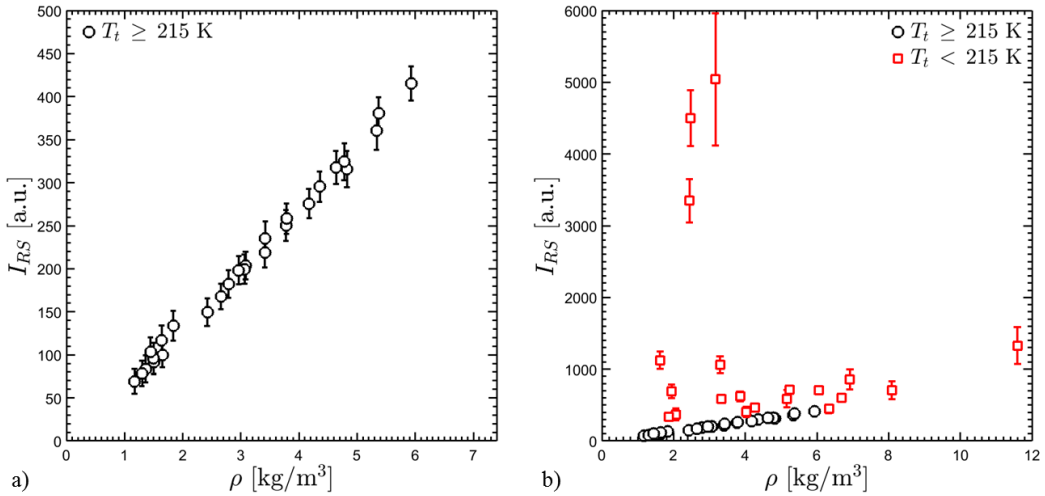

Figure 12. Rayleigh scattering intensity versus density. a) Data taken at total temperatures greater than or equal to 215 K and b) data taken over the entire facility operational envelope.

this phenomenon were reported in the previous two Rayleigh scattering attempts,[21,22] suggesting it is either a malfunction of the facility or is associated with the manner in which the current tests were conducted. Nonetheless, molecular Rayleigh scattering was collected over a broad range of the NASA Langley 0.3-m TCT facility, and was shown to vary linearly with the mass-density of the gas. Due to the issue experienced at lower temperatures, the range of utility is limited to total temperature conditions above 215 K for the present data.

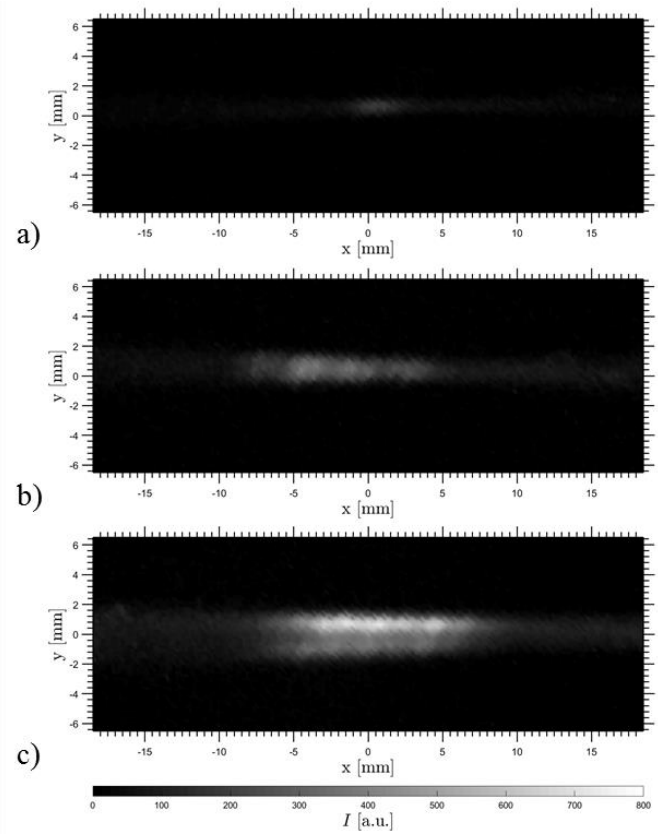

Figure 13. Comparison of mean Rayleigh scattering images at three different total temperature conditions, constant density, ρ = 3.35 kg/m^3. a) $T_t = 245$ K, b) $T_t = 133$ K, and c) $T_t = 100$ K.

B. Modeling the Thermodynamic Behavior

With the dependencies of the signal intensity and lifetime data established, a number of models can be constructed for use in evaluating the thermodynamic conditions in the facility. The modeling is all based on a small subset of the data taken within the facility, which is being termed the 'calibration set,' and consists of approximately 20 data sets (each containing approximately 2000 independent measurements) over the full tunnel operational envelope (all available P_t, T_t conditions). Though the values for the various modeling coefficients are given in the following sections, note that they are only valid for the present datasets and are not meant to suggest a universality to all data. However, the procedure and methodologies outlined are sufficiently general to be extended to other similarly collected data. As a final statement, only the ranges of validity established in Section IV.A are considered in the modeling so that physical effects not associated with the measurement technique itself are omitted.

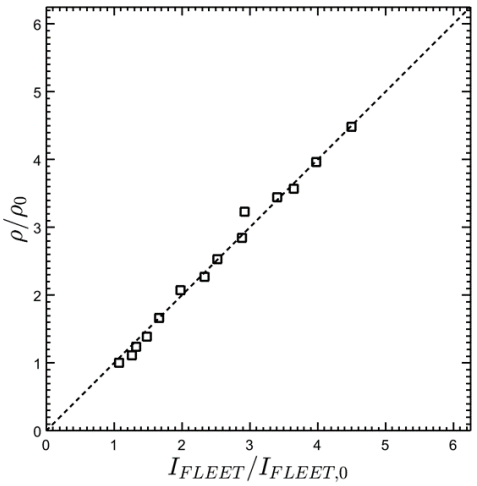

Figure 14. Comparison of FLEET signal intensity and density scaled with their reference values.

1. FLEET signal intensity

The FLEET signal intensity in the calibration data set was observed to vary linearly with the flow density. The simplest model to construct for this behavior is simply:

$$\frac{\rho}{\rho_0} = \frac{I}{I_0} \tag{4}$$

That is, assuming that the behavior is consistent, the changes in density should be directly proportional to the changes in intensity. The reference parameters, ρ_0 and I_0, were selected to be the first point in the calibration data set. The value of these two parameters for this data set are 1.17 kg/m^3 and 8.832×10^4 a.u., respectively (where ρ_0 corresponds to atmospheric density). The fit to the intensity data is shown in Fig. 14. As noted in Section IV.A.1, the measurements based on the FLEET signal intensity are limited to total temperatures above 167 K for the present data due to the misalignment of the femtosecond laser beam.

2. FLEET signal lifetime

There were two observed trends with the signal lifetime data. First, there was a strong density dependence, and second, the behavior was reminiscent of the collisional quenching of fluorescence. These observations suggests a number of paths forward for determining thermodynamic conditions from the signal lifetime. The lifetime, or two lifetimes, could be used to measure the density directly. Alternatively, the combined pressure/density/temperature dependence could be modeled, and with a secondary means of determining the density, the missing thermodynamic condition could be extracted from the model. To stay with convention in this discussion, rather than working with lifetimes decay rates shall be used instead: $\gamma_1 = 1/\tau_1$ and $\gamma_2 = 1/\tau_2$.

To model the density as a function of either decay rate requires a power-law fit. In this case the most practical approach used the following:

$$\frac{\rho}{\rho_0} = C_1 \left(\frac{\gamma}{\gamma_0}\right)^{-C_2} + C_3 \tag{5}$$

This is a purely empirical fit, and does not attempt to model any of the physical dependencies one would expect. Nonetheless, the fits constructed by this equation are sound, depicted in Fig. 15 with the underlying decay rates. The relevant fit parameters for these two empirical models are summarized in Table 1.

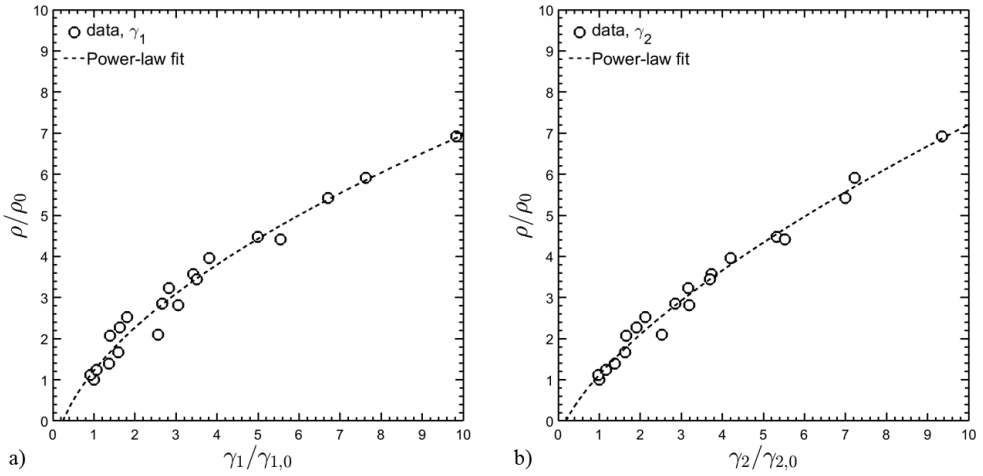

Figure 15. Density versus FLEET signal decay rates with power-law fit. a) γ_1 and b) γ_2.

Table 1: Power-law fit parameters for FLEET signal decay rates

Decay rate	ρ_0 [kg/m^3]	γ_0 [kHz]	C_1	C_2	C_3
γ_1	1.17	46.2	2.27	0.547	-1.05
γ_2	1.17	14.5	1.67	0.667	-0.549

A physical model can also be developed, which captures the behavior of the decay rates. Following the collisional quenching analogy, the total decay rate could be modeled as the sum of a 'natural' decay rate, which is independent of the collision rate of the molecules (though in this case it is likely a function of laser pulse energy and excitation wavelength), and an additional deexcitation rate associated with molecular collisions. Constructing a full model such as this requires not only accurate measurements of the thermodynamic conditions, but also the constitutive species present when the measurement was taken. Such analysis is simply not possible with the current datasets. However, a similar model can be constructed, which amalgamates the behavior of these different terms. The proposed model is of the form:

$$\gamma = D_1 + D_2 \left(\frac{P}{P_0}\right)^{D_3} \left(\frac{T}{T_0}\right)^{D_4} \tag{6}$$

In a traditional collisional quenching model, the coefficient D_3 should equal unity, and the temperature dependence comes from density effects, the mean collisional velocity, and the collisional quenching cross-section. The fit of this model to the present data is shown in Fig. 16; γ_1 and γ_2 are shown in Figs. 17a and 17b, respectively.

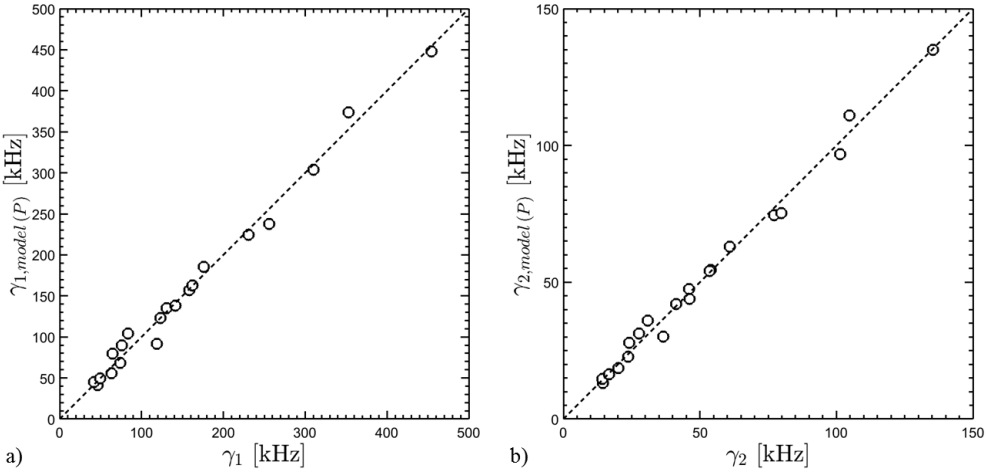

Figure 16. Comparison of pressure-based empirical fits to FLEET signal decay rates. a) γ_1 and b) γ_2.

A similar model can be constructed using density instead:

$$\gamma = D_1 + D_2 \left(\frac{\rho}{\rho_0}\right)^{D_3} \left(\frac{T}{T_0}\right)^{D_4} \tag{7}$$

The density-based fits for the signal decay rates are given in Figs. 18a and 18b, while the fit parameters for both the density- and pressure-based fits are summarized in Table 2. When modeled with respect to density, it can be seen that the temperature dependence (D_4) becomes quite small, particularly for the γ_2 case. This further supports the notion that the observed changes in the FLEET signal decay rates/lifetimes are exclusively a density effect, at least within these temperature and pressure domains. While using the physical models may help illuminate subtle thermodynamic dependences, it is questionable whether doing so provides utility in making a thermodynamic measurement. In particular, since the density effect is so dominant, there is likely little sensitivity to temperature when applying the model. This is discussed in further detail in Section IV.C. Finally, both the physical model and the power-law fits, since they are based on the signal lifetime, are applicable over the full operational range of the tunnel for these data sets.

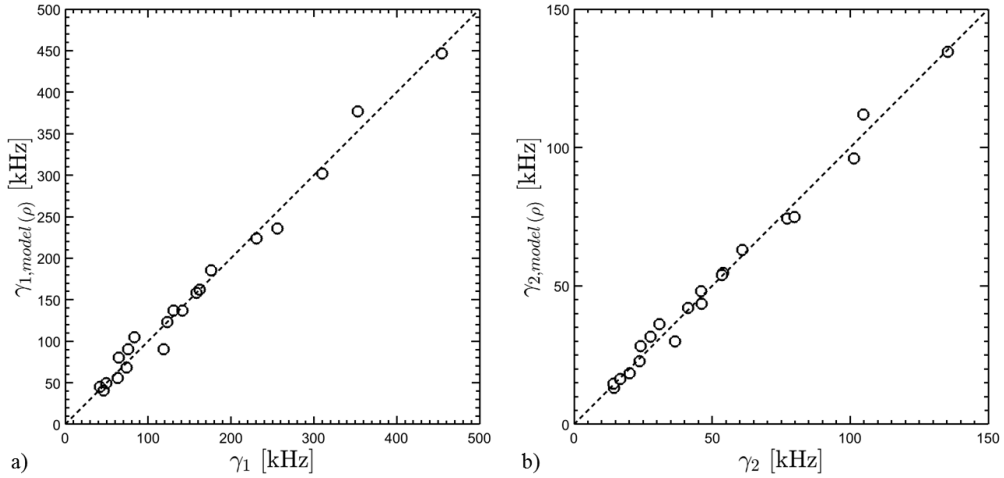

Figure 17. Comparison of density-based empirical model with FLEET signal decay rates . a) γ_1 and b) γ_2.

Table 2. Summary of fit parameters for physical empirical model

Decay rate	ρ_0 [kg/m^3]	P_0 [kPa]	T_0 [K]	D_1 [kHz]	D_2 [kHz]	D_3	D_4
γ_1	n/a	85.8	247	22.9	18.2	1.56	-1.82
	1.17	n/a	247	21.4	19.5	1.52	-0.203
γ_2	n/a	85.8	247	4.90	8.30	1.40	-1.52
	1.17	n/a	247	4.28	8.88	1.36	-0.076

3. Rayleigh scattering signal intensity

Section IV.A.3 demonstrated that, over a limited range of the tunnel operating conditions, the Rayleigh scattering signal intensity was directly proportional to the nitrogen density. This same trend can potentially be used to serve a measurement of density. Since it too followed a linear dependence, the same equation used to model the FLEET signal intensity data (Eq. 5) can be used to model the Rayleigh scattering. The resulting fit is presented in Fig. 18. The relevant fit parameters are: ρ_0 = 1.17 kg/m^3 and $I_{0,RS}$ = 69.3. As noted in Section IV.A.3, the range of applicability for the Rayleigh scattering measurements in this data set are all total temperatures greater than 215 K, so this graph contains fewer points than the previous ones.

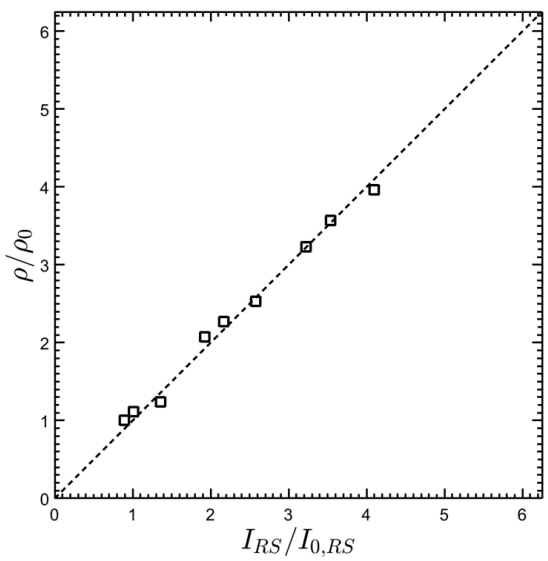

Figure 18. Comparison of Rayleigh scattering intensity with density, scaled against reference values.

C. Estimation of Tunnel Operating Conditions

This section discusses the accuracy and precision of thermodynamic measurements made using the models discussed in the previous section. These measurements utilize all data acquired across the tunnel operating conditions, rather than just the calibration set used in constructing the models.

1. Static Density

As discussed in the previous section, both the signal intensities and the FLEET signal lifetimes were quite sensitive to density. Consequently there are a number of ways to measure the density from the different models; there are a total of four methods available from the thermodynamic models that were developed in the previous section. Refer to Appendix B for an in-depth discussion of the methodologies involved in each of these approaches.

A comparison of the density measurements made using the FLEET signal intensity data with the measurements made by the facility DAS is shown in Fig. 19a. The predictive agency of this method is limited principally by the total temperature range discussed in Section IV.A.1. If only the data taken at total temperatures in excess of 167 K are considered, the mean standard error (in comparison to the DAS measurements) is 5.26 percent across all densities. Moreover, the mean measurement precision, herein defined as one standard deviation from the probability density function generated at each measurement point, was approximately 10 percent, though this does vary from set to set. A similar assessment can be made using the Rayleigh scattering measurements; a comparison with the facility DAS is shown in Fig. 19b. Again, the primary limitation to this measurement technique is the available total temperature range (above 215 K for the Rayleigh scattering measurements per Section IV.A.3). Above this demarcation, the mean standard error is within 3.55 percent, while the measurement precision here was again found to be approximately 10 percent.

The FLEET signal lifetime provided two separate routes for measuring the gaseous density. The first method is based on the empirical power-law fit from Section IV.B.2; a comparison of these measurements with those of the facility DAS are presented in Fig. 19c. Unlike the intensity-based measurements, the decay-rate-based measurements are possible over the entire total temperature range of the facility. The mean standard error for these data was found to be approximately 6.6 percent, and the measurement precision was approximately 12 percent. It should also be stated that at the lowest total temperature condition, the measurement precision was notably worse (approaching nearly 26 percent at the highest-density condition). Finally, a second method is available to measure the density from the FLEET signal decay rates. This method utilized information from both measured decay rates and the model equations (Eq. 7) to directly solve for the density. The measurements made in this manner are shown in comparison to the facility DAS measurements in Fig. 19d. These results are very similar to those made with power-law fit. Again, the applicable temperature range is the full tunnel operational envelope. The measured standard error was on average 7.2 percent, while the mean precision was approximately 10 percent. A summary of these four different density measurement techniques is shown in Table 3.

Table 3: Comparison of different methods for calculating density. Only data within scope of model is considered.

Method	T_t range [K]	ε [%]	σ_ρ/ρ (mean) [%]	σ_ρ/ρ (min) [%]	σ_ρ/ρ (max) [%]
FLEET signal intensity	167 – 300	5.26	10.0	7.26	28.6
RS signal intensity	215 – 300	3.55	10.2	4.86	18.4
Decay rate power-law fit	100 – 300	6.62	12.3	5.91	25.9
Dual decay empirical fit	100 – 300	7.23	9.99	6.31	20.9

Assessing these measurements in a broader context is difficult due to the unusual temperature and pressure conditions in which the measurements were being made. Inferred density measurements in similar conditions made by Woodmansee et al. using high-resolution N_2 coherent anti-Stokes Raman spectroscopy (CARS) in a lab-scale

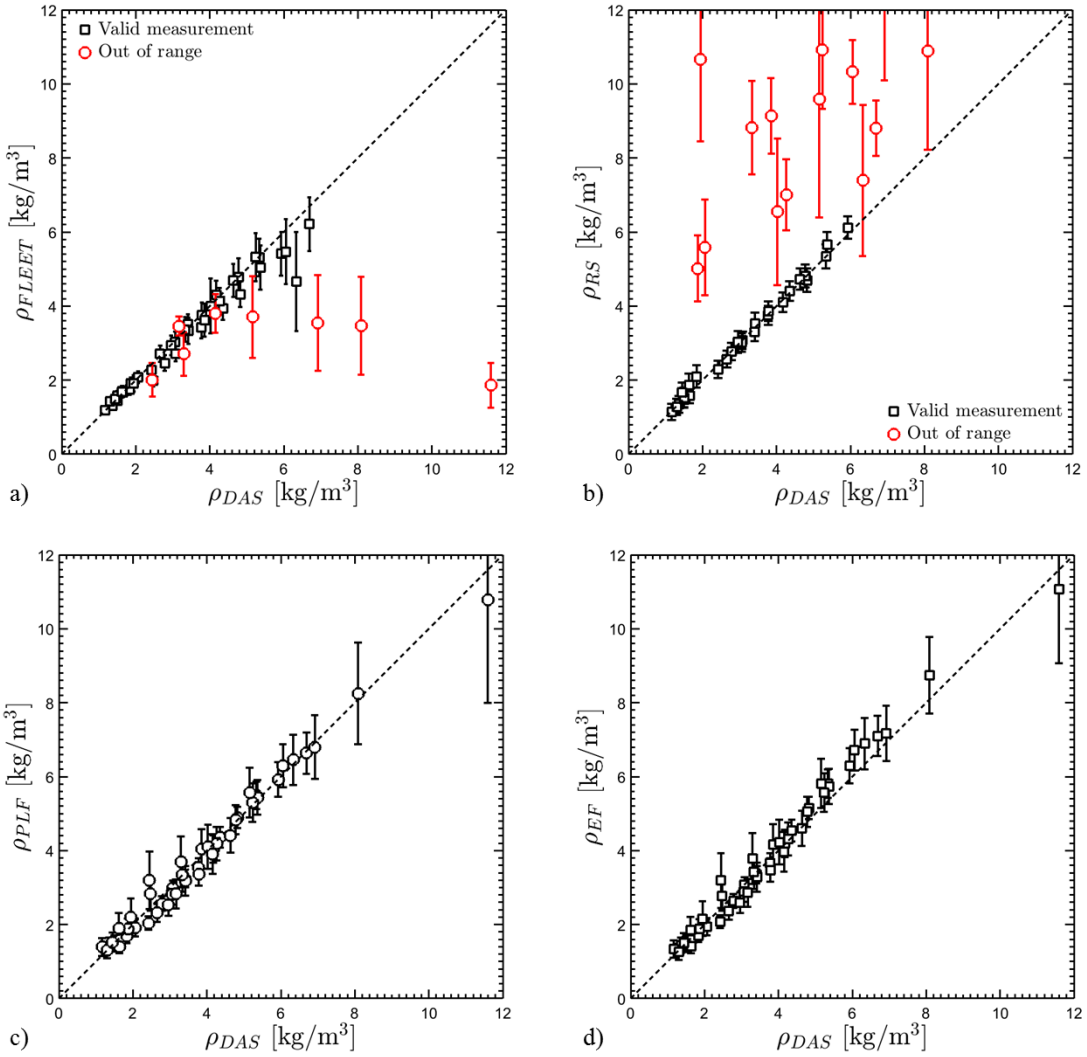

Figure 19. Comparison of density measurements with facility DAS. a) FLEET signal intensity, b) RS signal intensity, c) FLEET decay rate power-law fit, and d) FLEET dual decay rate.

underexpanded jet showed a few percent error (not stated overtly) when comparing their measurements to a theoretical distribution, and precisions ranging from between 4 to 10 percent.[25] Density measurements made via nitric oxide laser-induced fluorescence by Gross et al. operated with a measurement uncertainty of 2 percent in a moderate pressure, low temperature flow (Mach 2 turbulent boundary layer).[26] Filtered Rayleigh scattering (FRS) experiments of Forkey et al. [27] showed total measurement uncertainties of approximately 5 percent in measuring gaseous densities. Additionally, absolute molecular density measurements made by Balla and Everhart in a low-temperature Mach 10 flow yielded precisions between 32 and 6 percent, with the larger imprecision occurring at the lowest densities.[28] Ultimately, though the conditions under which the measurements were made were not identical, similar accuracies and precisions were observed with these density measurements as were those made with other optical diagnostics.

The measurements statistics in Table 3 suggest certain limitations to the applications of these density measurement techniques. The most obvious of these is the applicable total temperature range. This particular point is not anticipated to be a recurring problem for the measurement techniques; a simple engineered solution to properly accommodate the contraction of the tunnel would eliminate this cap on the measurement techniques. Perhaps a greater concern is the precision with which the measurements can be made. Typical transonic flows (in particular wakes and boundary layers) do not show the significant (order of magnitude) density changes observed in supersonic and hypersonic flows. For example, the wake behind a transonic body may show a density variation between 8 and 10 percent of the nominal freestream value. As a consequence, a higher precision is desirable since it would allow these subtle density changes

to be identified. With the current measurement precision, it is unclear whether sufficient sensitivity exists to detect a subtle density change as described. The imprecision stems from varying sources. In the case of the FLEET signal intensity, the imprecision is a result of the shot-to-shot variability in the laser pulse energy. Since the signal intensity is nonlinearly dependent on the pulse energy, an exaggerated variability is imparted to the intensity measurement, leading to a more imprecise density measurement. The Rayleigh scattering signal intensity similarly suffers from variability in the laser pulse energy. Additionally, the presence of extraneous scatterers in the facility (mostly random bits of dust and debris trapped in the flow-conditioning screens that are liberated during tunnel operation), add an extra unsteadiness to these measurements, which unfavorably biases the measurement precision. Though care was taken in the data reduction, accounting for every such occurrence in the large ensembles of data was an impracticality.

The lifetime-/decay-rate-based measurements are instantaneously quite susceptible to the laser intensity variations as well. While the lifetimes are self-normalizing in intensity, they are weak functions of the exciting laser energy. One report in the literature by DeLuca et al.[19] suggested a $1/e$ lifetime of nearly 150 μs when using a 6 mJ/pulse (approximately an order of magnitude more energy than that used in the present study), which is several times the duration of the longest $1/e$ lifetimes recorded in the present studies. Thus, while dependence of the FLEET signal lifetime(s) is not as strong as that of the initial FLEET signal intensity, some sensitivity to the shot-to-shot intensity variations should be expected. Moreover, the two measured decay rates vary differently with the laser energy, adding a further degree of imprecision to the measurements. An additional effect observed in more recent measurements by the authors (though not necessarily applicable in these studies) suggest the lifetime of the FLEET signal is also very sensitive to the local *strain rate* of the gas. Thus, it ultimately may prove impractical to try to isolate the thermodynamic effects from all the various factors that influence the lifetime of the FLEET signal, except in special circumstances.

As a final note about the density measurements, corrections could, in principle, be made to correct for the intensity variations in the Rayleigh scattering measurements (and potentially the FLEET intensity measurements if a sufficiently robust model of the intensity dependence is established). For example, the shot-to-shot intensity variations could be measured with a photodiode, and subsequently a scaling factor applied to correct the image. Such a correction might improve the measurement precision by a factor of two or more. Furthermore, relative density measurements could still be made with a higher degree of precision. If the FLEET or Rayleigh scattering were done along a line or plane (rather than a point or integrated measurement, as presented here), the same intensity fluctuations are experienced everywhere in the image. Thus, if the density is known to a high degree of precision at one place along the line or plane, the single-shot measurements would likely exhibit far less variability than the uncorrected ensembles in the present studies.

2. Static Temperature

There are numerous means of numerically calculating the static temperature of the flow based on the decay rate models in Section IV.B. For example, one of the density measurements from Section IV.C.1 could be used in conjunction with Eq. 7 to evaluate the temperature. Alternatively, one of the two decay rates could be used along with a measured density and an appropriate equation of state (Beattie-Bridgeman EOS in this case) to evaluate the temperature and pressure simultaneously through Eq. 6 (discussed in Appendix B). The temperature measurements made in this manner are presented in Fig. 20a. Despite the various numerical pathways leading to these measurements, each ultimately suffers from the same limitation. The FLEET signal decay rates are strong functions of the density while exhibiting only weak orthogonal dependence on the temperature. For a perfect density measurement (100 percent accuracy and 0 precision) and perfect model, this wouldn't be a limiting factor. However, the low (10 percent) precision of the density measurements combined with the moderate accuracy completely overshadow the weak temperature sensitivity. As a result, the temperature distributions calculated at each set of conditions are nearly uniform, yielding little but fortuitous accuracy to the true temperature. Consequently, as a *direct* measurement of temperature, the current FLEET data is insufficient.

However, the FLEET data enable an alternative means of measuring the temperature. Along with the density information that the signal intensity and lifetimes yield, FLEET is simultaneously measuring the velocity. As a result, with only weak assumptions, an accurate measurement of the temperature can be made *indirectly*. One way of making this measurement is to assume that the total temperature (or less strongly that the total enthalpy) of the flow is constant. Doing so, the temperature can be expressed as:

$$T = T_t + \frac{1}{2}\frac{\|u\|^2}{c_p(\rho, T)} \tag{8.1}$$

$$h(\rho, T) = h_t(\rho_t, T_t) - \frac{1}{2}\left|\left|u\right|\right|^2 \tag{8.2}$$

The density used in these calculations were taken from the dual decay empirical fit, while the $||u||$ term is the absolute magnitude of the velocity vector. The results for the calculations using the isenthalpic assumption are shown in Fig. 20b. The temperatures measured in this way are found to be in agreement with the facility DAS. In this case, the mean standard error across all conditions is 0.62 percent, while the mean precision is found to be 0.26 percent. A comparison between the two temperature measurements presented here is given in Table 4.

Table 4: Comparison of different methods for calculating static temperature.

Method	T_t range [K]	ε [%]	σ_T/T (mean) [%]	σ_T/T (min) [%]	σ_T/T (max) [%]
γ_{EF} + EOS + ρ	100 – 300	40.4	28.9	16.9	54.9
$(h_t = const.)$ + ρ + u	100 – 300	0.62	0.26	0.03	2.46

In evaluating the temperatures measured using the constant total enthalpy assumption, it is important to understand that, first, the accuracy and precision are results primarily of the accuracy and precision of the velocity measurements. The specific heat of the gas is a weak function of the density, and so the comparatively large error and precision of the density measurement do not have a drastic influence on the resulting temperature measurement. Second, the assumption of constant total enthalpy requires an independent measurement of the total conditions (temperature and density/pressure) for calibration. In this case, the facility DAS provided the additionally necessary data, as most facilities could. However, this action makes the measurement more dependent on the facility DAS measurements, which, if they are the quantity in question, undermines the utility of the measurements in some capacity. Furthermore, while not a particularly strong assumption, it is quite simple to invalidate the assumption of constant total enthalpy. For instance, having a test section with slotted walls (with gas being exchanged between the plenum and test section) or injecting a gas of differing enthalpy quickly makes these temperature measurements dubious. Operating the facility while thermodynamic conditions are changing could also invalidate this assumption in certain circumstances. Furthermore, particular classes of flows (shear flows, for example) also have viscous heating and thermal diffusion, which are not directly accounted for in this assumption. However, important types of flows in the transonic regime would still permit these velocity measurements. For example shockwaves present on transonic bodies could be assessed for changes in temperature and velocity. The measurement of temperatures above bodies with a large degree of curvature, such at airfoils at high angles of attack, could be made provided the measurements were made in the primarily inviscid regions of the flow. Thus, there is still value in assessing the measurements made in this fashion.

These limitations aside, accurate measurements of the temperature were possible using the FLEET data. For comparison, the temperature measurements by made using high-resolution N_2 CARS in an underexpanded jet by Woodmansee et al. were found to have high accuracy (when compared to CFD) and precisions as low as 5 K or approximately 2.5 percent of the measured temperature.[29] Previous temperature measurements using FLEET, which based the thermometry on the fitting of rotational spectra in the ultraviolet portion of the emission, found uncertainties

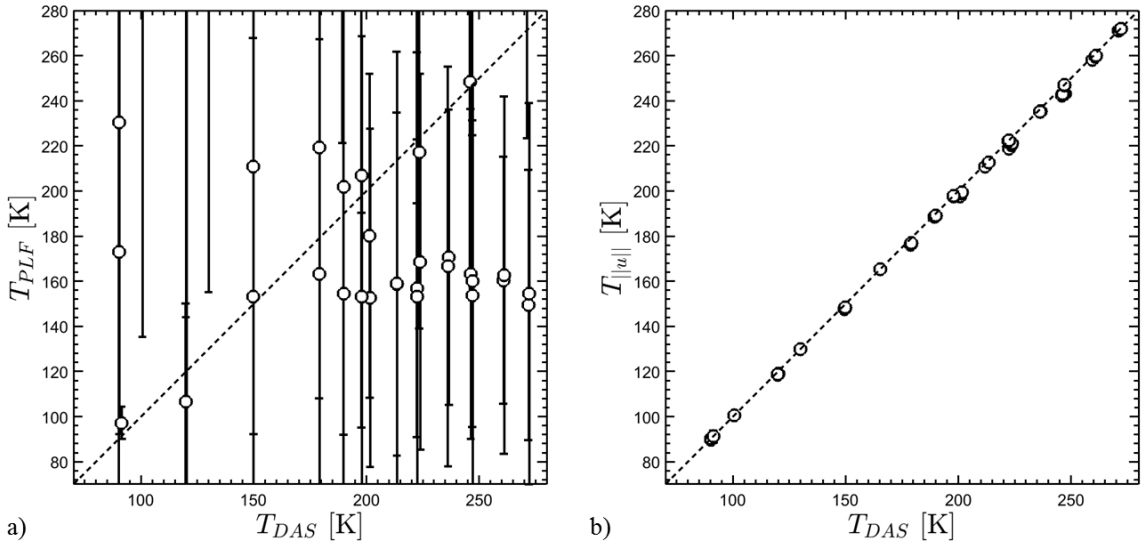

Figure 20. Comparison of temperature measurements with those by the facility DAS. a) Direct measurement and b) measurement assuming constant total enthalpy (error bars are present but hidden by the data points).

between 20 and 50 K for high-temperature measurements, though there was an overall bias to the measurements due to the localized heating of the gas by the femtosecond laser pulse. Simultaneous temperature and pressure measurements by Kearney and Danehy, which utilized hybrid femtosecond/picosecond CARS at elevated pressures, were found to exhibit marked accuracy in temperature, within 1 percent, along with precision ranging from 0.7 to 1.4 percent.[30] Filtered Rayleigh scattering (FRS) measurements made by Forkey et al. showed a temperature measurement uncertainty of approximately 3 K or 2 percent at standard to slightly elevated pressures.[27] Mielke et al. found lower-bound temperature uncertainties of 58 K or approximately 20 percent with interferometric Rayleigh scattering measurements, though higher accuracy was claimed in RMS fluctuation measurements using noise-floor subtraction.[31] Finally, very precise measurements of temperature were made through laser-induced thermal acoustics (LITA) by Hart et al., which showed temperature precisions within 0.3 percent and accuracies within 0.5 percent.[32] The measurements made with FLEET thus compare to or exceed the measurements previously made with similar and related techniques, with the caveat of needing a reference measurement for proper calibration.

3. Static Pressure

Direct measurement of the static pressure from the FLEET signal intensity/decay rate faces the same limitations as that of the static temperature; the decay rates are almost exclusively functions of the density. Consequently, the sensitivity to temperature and thusly the pressure is limited. Despite numerous pathways through to the measurement of pressure, the results are not particularly encouraging. The results of one such method, calculated simultaneously with the direct temperature measurement described above and in Appendix B, are shown in Fig. 21a. Much like the related temperature measurement, the single-shot pressures calculated in this fashion suffer from broad probability distributions and inaccurate means.

The same alternative route is available for the static pressure as for the temperature; by assuming a constant total enthalpy and using the single-shot velocity measurements to evaluate the temperature, the static pressure can be calculated with an experimentally determined density measurement (FLEET or otherwise) and using an equation of state (Beattie-Bridgeman equation in these studies). Since the thermodynamic state of the gas can be defined through any two state variables (for non-reacting flows), the final condition (in this case pressure) is uniquely determined through the EOS. The results of these calculations are shown in Fig. 21b, based on the density measurements made with a power-law fit to the FLEET signal lifetime (to cover the entire temperature range). The pressures measured in this fashion are far more representative of those measured by the facility DAS than those depicted in Fig. 21a. The mean standard error is, on average, approximately 6 percent, while the mean precision is 10.7 percent. Not surprisingly, these figures are very similar to the accuracy and precision of the density measurement that the data on which it is based. A comparison of these two measurement methods is given by Table 5.

Pressure measurements with similar or higher accuracy and precision are fairly common throughout the literature. The high-resolution N_2 CARS by Woodmansee et al. found that the accuracy of their pressure measurement varied depending on the pressure itself. Notably, at sub-atmospheric pressures, the CARS measurements typically over-

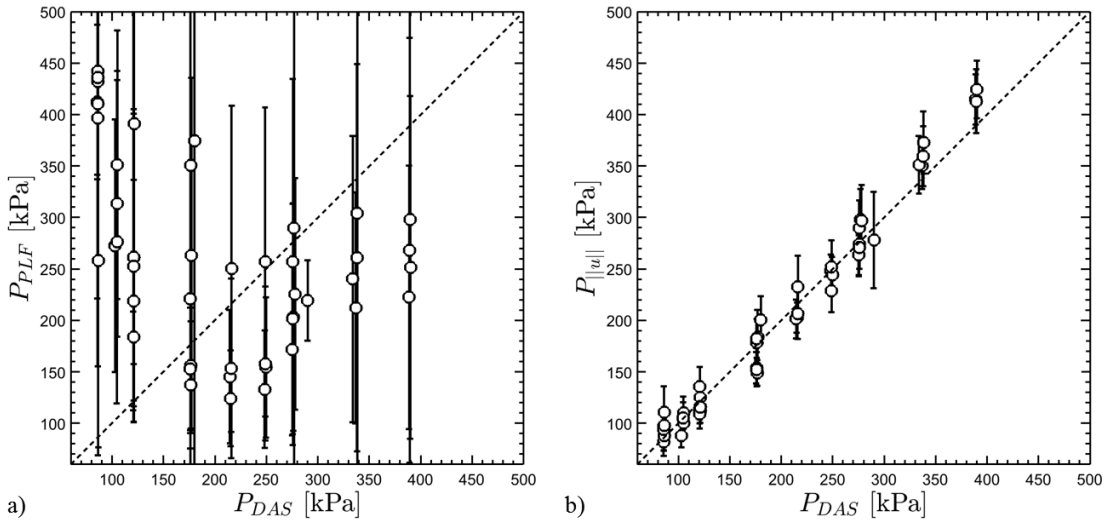

Figure 21. Comparison of static pressure measurements with those measured by the facility DAS. a) Direct measurement using FLEET thermodynamic models and b) measurement assuming a constant total enthalpy.

predicted the pressure, while under-predicting at higher pressures. Overall, a systematic bias of 4 percent was present at the pressure range applicable to these studies.[29] Gross et al., using a nitric oxide LIF-based technique, were able to make pressure measurements with a precision as high as 2 percent, attributed mostly to instrumental noise levels.[26] The accuracy of hybrid femtosecond/picosecond cars by Kearney and Danehy were found to be as high as 2 percent, though there was a strong dependence on the measurement probe delay time. The precision of these same measurements was found to be a function the absolute pressure being measured in addition to the same probe delay time to which the accuracy was sensitive.[30] Pressure measurements by Hart et al. using LITA in a supersonic wind tunnel reported approximately 4 percent across all measured pressures, though these measurements were all at greatly reduced pressures.[33] Finally, the FRS measurements by Forkey et al. showed a total measurement uncertainty between 4 and 5 percent at ambient to slightly elevated pressures.[27]

While the present ability to measure pressure with the FLEET technique still lags behind some of the above examples, this demonstration of the measurement ability is still encouraging. It must be stated that much as the temperature measurements based on the isenthalpic assumption suffer from physical limitations, the pressure measurement lacks utility in the same fashion. That is, shear flows, injectant flows, and non-adiabatic flows cannot be evaluated without caveat. However, one relevant flow scenario that is not invalidated through this assumption are flows with shockwaves. For example, the thermodynamic and velocity fields could be mapped out in the inviscid region over a transonic airfoil with a shock situated at some position on the chord. With the current level of precision and accuracy, the minimum threshold for measuring changes in conditions across a shock is a local Mach number of approximately 1.05. Thus, though there are certain limitations placed on the validity of the measurements, the ability of FLEET to make off-body measurements of interest is still quite encouraging.

Table 5: Comparison of different methods for calculating static pressure.

Method	T_t range [K]	ε [%]	σ_P/P (mean) [%]	σ_P/P (min) [%]	σ_P/P (max) [%]
γ_{EF} + EOS	100 – 300	44.3	27.2	15.5	46.7
$(h_t = const.)$ + EOS	100 – 300	6.20	10.7	6.13	20.6

D. Discussion

All of the measurements, modeling, and analysis in the previous sections are meant to outline a methodology that could make possible the measurement of thermodynamic conditions with FLEET and RS data. Previously, FLEET has not thoroughly been evaluated for its ability to measure thermodynamic conditions in a large-scale facility or at the conditions observed in these studies (high pressure, low temperature). It was thus unclear whether the technique could serve as a clear metric of any quantity other than velocity in this context. However, it has now been demonstrated that the density could be measured with reasonable accuracy and precision using the FLEET signal alone or by using the Rayleigh scattering signal. These measurements do require a few data points for calibration, but are able to maintain their integrity without further assumption.

As was demonstrated, the direct measurement of the other thermodynamic quantities proved difficult. The fundamental reason for this occurrence was the lack of temperature sensitivity in the FLEET signal lifetimes. As a result, the imprecision and inaccuracy of the density measurements lead to much larger discrepancies in the associated temperature measurement. Thus, at face value, only a density measurement could be reasonable extracted from these data without further information. However, making the assumption of constant total enthalpy is not unreasonable for many situations in this type of facility. Operationally, before data are collected, the facilities are run at the desired test conditions to assure that the models and walls of the test section come into thermal equilibrium with the gas in the test section. Consequently, it is not an unreasonable assumption to make when measuring freestream conditions. However, when a slotted test section is involved, or if secondary injection of gases is being conducted, its validity is diminished. Another possible way forward with temperature measurement is the spectral measurement of the FLEET signal. As was noted above, the attempts at making temperature measurements in this way have contained measurement bias due to the localized heating of the gas by the absorption of the laser pulse (up to several hundred K). A new variant of FLEET, selective two-photon absorptive resonance FLEET (STARFLEET),[34] shows promise at avoiding this issue by depositing substantially less (orders of magnitude) energy into the gas. Indeed, the preliminary spectral measurements indicated a local temperature rise of only 10 to 20 K in these studies.

An important point that has not been mentioned yet is the *experimental simplicity* of using these techniques. Both FLEET and RS are single laser, single camera techniques, do not require spectral dispersion of the signals or tuning of their laser source (or multiple laser sources), and have relatively straightforward (though time consuming) data processing. Throughout the results, comparisons with techniques such as CARS, LITA, and filtered or interferometric Rayleigh scattering were given to keep the measurements made in context. However, these techniques pose

significantly greater experimental challenges in TCT-type facilities. Thus, even if superior measurements were possible in lab environments, it is highly questionable whether such improvements would translate over to operating in large-scale facilities. Overall, the results of these studies were very encouraging. Off-body measurements of both velocity and thermodynamic condition were made, whether directly or indirectly. A summary of the results for the different measurements elaborated in this paper are given by Table 6. Further studies are necessary to validate these trends and assess whether the framework heretofore outlined could be further refined.

Table 6: Summary of Highest Measurement Accuracy and Precision for different quantities

Quantity	T_t domain [K]	P_t domain [kPa]	ε [%]	σ_n/n [%]
Velocity	100 – 300	100 – 400	1.48	0.73
Density (FLEET, PLF)	100 – 300	100 – 400	6.62	12.3
Density (RS)	215 – 300	100 – 400	3.55	10.2
Temperature	100 – 300	100 – 400	0.62	0.26
Pressure	100 – 300	100 – 400	6.20	10.7

V. Conclusions

Femtosecond laser electronic excitation and tagging (FLEET) and molecular Rayleigh scattering were studied for their thermodynamic dependencies in the NASA Langley 0.3-m TCT facility. The intensity of the FLEET and Rayleigh scattering signals were found to be directly proportional to the gas density in which they were induced, while the lifetime and decay rate of the FLEET signal was found to have a strong density dependence and a mild temperature dependence. These behaviors were used to construct physical and empirical models of the behavior of the technique. Subsequently, these model equations were used to measure the conditions within the tunnel freestream. Density, temperature, and pressure were measured by FLEET with accuracies of approximately 7 percent, 0.6 percent, and 6 percent, respectively. The precision of these measurements were similarly diverse: the density precision were roughly 10 percent, temperature approximately 0.3 percent, and pressure 11 percent. Density measurements using Rayleigh scattering showed a slightly higher accuracy of 3.5 percent and similar precision. These measurements indicate that both FLEET and Rayleigh scattering could potentially serve as thermodynamic measurement techniques for evaluating and assessing freestream flow conditions as well as certain transonic flows of interest.

Appendices

A. Linearity of high-speed CMOS camera

One crucial aspect in evaluating the thermodynamic dependences of the FLEET signal intensity and lifetime is the linearity of the high-speed CMOS camera. That is, it is implicitly assumed that the camera responds in a controlled and repeatable fashion to varying levels of signal intensity. The manufacturers provided no linearity specification for the camera used in these studies, and so its behavior had to be characterized over the full range of intensities.

Methodologically, this was achieved by observing the FLEET signal at different intensities. First, the gain on the image intensifier was gradually increased such that the FLEET signal just barely saturated the CMOS sensor. A series of images were then captured at each of the aperture settings on the collection lens ($f/2, f/2.8, f/4, f/5.6, f/8, f/11$, and $f/16$). Several sets like this were then taken at different intensifier gains. The peak intensities of the means of these sets were then compared to the relative aperture settings, allowing for the camera response to be evaluated as a function of the incident intensity. The results of these studies are shown in Fig A.1.

It is seen that camera's overall signal response was linear with respect to the intensity of the incident intensity. The maximum observed mean intensity was approximately 3300 counts out of 4095. Though the instantaneous signals often were near saturation, the degree of variability in the FLEET signal made setting the gain at the top end quite difficult, and to prevent saturation biasing at this intensity, the gain was kept lower. Nonetheless, the linear trend was quite consistent. The curves corresponding to different gains are all in roughly the same proportion to each other, indicating that the linearity was consistent over the full well of the sensor (note that a 1 percent change in gain corresponds to approximately a 15 percent change in signal). The only exception to this trend was near the noise floor of the camera, which was approximately 20 counts RMS at the time and settings used during these studies. Since no signal could be distinguished from the background at these intensities, it was not possible to establish linearity below

this threshold. Nonetheless, over the ranges of signals collected for these studies, the combined effect of the intesnifer and camera responded linearly.

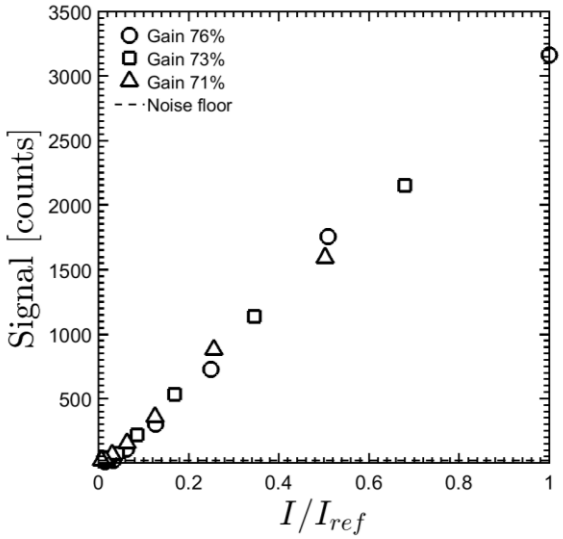

Figure A.1. Linearity data for high-speed CMOS sensor.

B. Density and Temperature measurement methodologies

This appendix details the different methodologies used in evaluating thermodynamic conditions using the models constructed in Section IV.B.

1. Static Density

The density could be evaluated in many different ways based on the model equations in Section IV.B. The density calculations based on the FLEET and Rayleigh scattering signal intensities were very straightforward; the model equation (Eq. 4) was rearranged minorly to directly yield the density from the measured intensity:

$$\rho_{FLEET,RS} = \rho_0 \frac{I}{I_0} \tag{B.1}$$

Thus, the calculation of density from either the FLEET signal intensity or the Rayleigh scattering signal intensity was a direct substitution based on the model equation.

Calculating the density based on the FLEET signal decay rates were more complicated. The first approach, based on the power-law fit, was a similarly direct substitution based on Eq. 5:

$$\rho_{PLF} = \rho_0 \left(C_1 \left(\frac{\gamma}{\gamma_0} \right)^{-C_2} + C_3 \right) \tag{B.2}$$

In the actual data presented in Section IV.C.1, a density was calculated based on each decay rate (γ_1 and γ_2), and then the mean of these two values were given.

The final method presented in Section IV.C.1, termed the 'dual decay empirical fit,' was based on Eq. 7. Since the two empirical decay rates are known for every data point, there is a unique density and temperature combination, which will give rise to the data. Thus, by justly assuming that T/T_0 is the same independent of which decay rate the fit applies to, the density can be measured by rearranging Eq. 7 with respect to T/T_0 for each of the decay rates, then setting them equal to one another. The resulting density can be expressed as:

$$\rho_{EF} = \rho_0 \left(\frac{\gamma_2 - D_{1,2}}{D_{2,2}\left(\left(\frac{\gamma_1 - D_{1,1}}{D_{2,1}} \right) \left(\frac{\gamma_2 - D_{1,2}}{D_{2,2}} \right)^{-D_{3,1}/D_{3,2}} \right)^{\frac{1}{D_{4,1} + D_{4,2}\frac{D_{3,1}}{D_{3,2}}}}} \right)^{\frac{1}{D_{3,2}}} \tag{B.3}$$

Here, the first subscript on the coefficients represents which term in Eq. 7 the parameter refers to while the second subscript represents whether it corresponds to γ_1 (1) or γ_2 (2). The reason this method works is because the thermodynamic dependencies of each model equation are sufficiently distinct to provide the necessary sensitivity to the measured decay rate.

2. Static Temperature

Much like the density, numerous paths exist for calculating the temperature from the measured quantities. However, only the two presented methods will be discussed in detail. The first method, which was based on Eq. 6, required an independent density measurement. While this could have come from any of the four presented methods discussed in the preceding section, the power-law fit method was selected for its (slightly) higher precision and ability to operate over the full range of tunnel conditions. The temperature and the pressure were then solved for simultaneously in iterative fashion. To achieve this, the temperature and pressure were first confined to vary in such a way as to be consistent with the Beattie-Bridgeman equation of state. The density measurement acted as the anchor to ensure that the measurement was physically consistent; if a temperature was defined, the pressure was automatically defined as well. Then Eq. 6 was evaluated for both decay rates, and the residual with each decay rate was calculated. The temperature was then varied, and a selection was made to minimize the collective residual between both of the measured decay rates and the predicted decay rates. The problem with this method was that it required a much higher level of precision (and possibly accuracy) in the density measurement to make it viable; the decay rates are very sensitive to changes in density compared to the temperature.

The second method utilized the assumption of a constant total enthalpy and an independent density measurement. Technically it also requires that the composition of the flow be constant as well, but since the tests were conducted in a pure nitrogen flow, this assumption wasn't considered relevant. These assumptions then directly relate the thermal and velocity fields through Eq. 8.2. The FLEET velocimetry is able to measure two components of velocity in the current setup; the magnitude of this velocity is considered to be the $||u||$ term in the same equation. The total enthalpy is then calculated through standard NIST relations for molecular nitrogen using the facility DAS measurements of total temperature and total density.[35] Finally, using the independent density and velocity data, the static temperature was iterated on until convergence was achieved, which was specified to be within 10^{-8} K.

3. Static Pressure

The results presented in Section IV.C.3 utilize two different methods for evaluating the static pressure of the gas. The first method was described in the preceding section, where the temperature and pressure were solved for simultaneously. The second method utilized the temperature measurement based on the velocity and density measurements; the temperature and density were directly substituted into the Beattie-Bridgeman equation of state to yield the static pressure. Ensembles of single-shot measurements were then populated for later analysis.

Acknowledgments

The authors would like to thank all of the expert staff at the NASA Langley 0.3-m TCT including Wes Goodman, Michael Chambers, Karl Maddox, Cliff Obara, Chris Cramer, Reggie Brown, and Gary Beachem. These test would not have been possible without the long hours and hard work everyone contributed. Additional thanks is given to Stephen Jones and Brett Bathel for their help in setting up the experiments. This work was funded by NASA Langley's IRAD program. Christopher Peters was supported by a NASA Space Technology Research Fellowship (NSTRF).

References

[1] Oberkampf, W.L., Trucano, T.G., and Hirsch, C., "Verification, Validation, and Predictive Capability in Computational Engineering and Physics," *Foundations for Verification and Validation in the 21st Century Workshop*, Laurel, MD, Oct 22-23, 2002.

[2] Duque, E.P.N., Imlay, S., Ahern, S., Chen, G., and Kao, D., "NASA CFD Vision 2030 Visualization and Knowledge Extraction: Panel Summary from AIAA Aviation 2015 Conference," *54th AIAA Aerospace Sciences Meeting*, San Diego, CA, Jan. 4-8, 2016.

[3] Ladson, C. L. and Ray, E. J. *Evolution, Calibration, and Operational Characteristics of the Two-Dimensional Test Section of the Langley 0.3-Meter Transonic Cryogenic Tunnel;* NASA Technical Paper 2749: Hampton, VA, 1987.

[4] Snow, W. L., Burner, A. W., and Goad, W. K., "Image Degradation in Langley 0.3-Meter Transonic Cryogenic Tunnel," *NASA Technical Memorandum 84550*, 1982, pp. 1-25.

[5] Snow, W. L., Burner, A. W., and Goad, W. K., "Improvement in the Quality of Flow Visualization in the Langley 0.3-Meter Transonic Cryogenic Tunnel," *NASA Technical Memorandum 87730*, 1987, pp. 1-24.

[6] King, R.A., Andino, M.Y., Melton, L., Eppink, J., and Kegerise, M.A., "Flow Disturbance Measurements in the National Transonic Facility," *AIAA Journal*, vol. 52, no. 1, pp. 116-130. 2014.

[7] Batill, S.M., "Experimental Uncertainty and Drag Measurements in the National Transonic Facility," *NASA CR 4600*, 1994.

[8] Igoe, W.B., "Analysis of Fluctuating Static Pressure Measurements in the National Transonic Facility," *NASA TP 3475*, 1996.

[9] Quest, J. and Konrath, R. "Accepting a Challenge - The Development of PIV for Application in pressurized cryogenic Wind Tunnels," *41st AIAA Fluid Dynamics Conference and Exhibit*, Honolulu, HI, 2011.

[10] Willert, C., Stockhausen, G., Beversdorff, M., Klinner, J., Lempereur, C., Barricau, P., Quest, J., and Jansen, U., "Application of Doppler global velocimetry in cryogenic wind tunnels," *Experiments in Fluids*, Vol. 39, 2005, pp. 420-430.

[11] Gartrell, L. R., Gooderum, P. B., Hunter, W. W., and Meyers, J. F., "Laser Velocimetry Technique Applied to the Langley 0.3-Meter Transonic Cryogenic Tunnel," *NASA Technical Memorandum 81913*, 1981, pp. 1-35.

[12] Honaker, W. C. and Lawing, P. L., "Measurements in the Flow Field of a Cylinder with a Laser Transit Anemometer and a Drag Rake in the Langley 0.3-m Transonic Cryogenic Tunnel," *NASA Technical Memorandum 86399*, 1985, pp. 1-24.

[13] Fey, U., Konrath, R., Kirmse, T., Ahlefeldt, T., Kompenhans, J., and Egami, Y., "Advanced Measurement Techniques for High Reynolds Number Testing in Cryogenic Wind Tunnels," *48th AIAA Aerospace Sciences Meeting Including the New Horizons Forum and Aerospace Exposition*, Orlando, FL, 2010, pp. 1-8. AIAA-2010-1301.

[14] Watkins, A.N., Leighty, B.D., Lipford, W.E., Oglesby, D.M., Goodman, K.Z., Goad, W.K., Goad, L.R., Massey, EA., "The Development and Implementation of a Cryogenic Pressure Sensitive Paint System in the National Transonic Facility," *47th AIAA Aerospace Sciences Meeting including The New Horizons Forum and Aerospace Exposition*," Orlando, FL, 2009, pp. 1-10, AIAA-2009-421.

[15] Abram, C., Fond, B., Heyes, A.L., and Beyrau, F., "High-sped planar thermometry and velocimetry using thermographic phosphor particles," *Applied Physics B*, 111. pp. 155-160, 2013.

[16] Michael, J. B., Edwards, M. R., Dogariu, A., and Miles, R. B., "Femtosecond laser electronic excitation tagging for quantitative velocity imaging in air," *Applied Optics*, Vol. 50, No. 26, 2011, pp. 5158-5162.

[17] Burns, R.A., Danehy, P.M., Halls, B.R., and Jiang, N., "Application of FLEET Velocimetry in the NASA Langley 0.3-Meter Transonic Cryogenic Tunnel," *31st AIAA Aerodynamic Measurement Technology and Ground Testing Conference*, Dallas, TX, 2015, AIAA-2015-2566.

[18] Edwards, M.R., Dogariu, A., and Miles, R.B., "Simultaneous Temperature and Velocity Measurements in Air with Femtosecond Laser Tagging," *AIAA Journal*, Vol. 53, No. 8, 2015, pp. 2280-2288.

[19] DeLuca, N.J., Miles, R.B., Kulatilaka, W.D., Jiang, N., Gord, J.R., "Femtosecond Laser Electronic Excitation Tagging (FLEET) Fundamental Pulse Energy and Spectral Response," *30th AIAA Aerodynamic Measurement Technology and Ground Testing Conference*, Atlanta, GA, 2014, pp. 1-7.

[20] Eckbreth, A.C., *Laser Diagnostics for Combustion Temperature and Species*. 2nd ed., Gordon and Breach Science Publishers, 1996, Chap. 5.

[21] Shirinzadeh, B., Herring, G. C., and Barros, T. "Demonstration of Imaging Flow Diagnostics Using Rayleigh Scattering in Langley 0.3-Meter Transonic Cryogenic Tunnel," *NASA Technical Note 1999-208970*, Hampton, VA, 1999.

[22] Herring, G.C. and Shirinzadeh, B., "Flow Visualization of Density in a Cryogenic Wind Tunnel Using Planar Rayleigh and Raman Scattering," *NASA TM-2002-211630*, 2002.
[23] Beattie, J.A. and Bridgeman, O.C., "A New Equation of State for Fluids," *Proceedings of the American Academy of Arts and Sciences*. Vol. 63, No. 5, 1928, pp. 229-308.
[24] Michael, J.B., Edwards, M.R., Dogariu, A., and Miles, R.B., "Velocimetry by femtosecond laser electronic excitation tagging (FLEET) of air and nitrogen," *50th AIAA Aerospace Sciences Meeting including the New Horizons Forum and Aerospace Exposition*, Nashville, TN, 2012, pp. 1-8.
[25] M. Woodmansee, J. Kuehner, R. Lucht, and J. Dutton. "Pressure, temperature, and density measurements using high-resolution N2 CARS," *34th AIAA/ASME/SAE/ASEE Joint Propulsion Conference and Exhibit*, Cleveland, OH, 1998, pp. 1-15.
[26] Gross, K.P., McKenzie, R.L., and Logan, P., "Measurements of temperature, density, pressure, and their fluctuations in supersonic turbulence using laser-induced fluorescence," *Experiments in Fluids*, Vol. 5, 1987, pp. 372-380.
[27] Forkey, J.N., Lempert, W.R., and Miles, R.B., "Accuracy limits for planar measurements of flow field velocity, temperature and pressure using Filtlered Rayleigh Scattering," *Experiments in Fluids*, Vol. 24, 1998, pp. 152-162.
[28] Balla, R.J., and Everhart, J.L., "Rayleigh Scattering Density Measurements, Cluster Theory, and Nucleation Calculations at Mach 10," *AIAA Journal*, Vol. 50, No. 3, 2012, pp. 698-707.
[29] Woodmansee, M.A., Lucht, R.P., and Dutton, J.C., "Development of high-resolution N_2 coherent anti-Stokes Raman scattering for measuring pressure, temperature, and density in high-speed gas flows," *Applied Optics*, Vol. 39, No. 33, 2000, pp. 6243-6256.
[30] Kearney, S.P. and Danehy, P.M., "Pressure measurements using hybrid femtosecond/picosecond rotational coherent anti-Stokes Raman scattering," *Optics Letters*, Vol. 40, No. 17, 2015, pp. 4082-4085.
[31] Mielke, A.F., Elam, K.A., and Sung, C.J., "Multiproperty Measurements at High Sampling Rates Using Rayleigh Scattering," *AIAA Journal*, Vol. 47, No. 4, 2009, pp. 850-862.
[32] Hart, R.C., Balla, R.J., and Herring, G.C., "Simultaneous velocimetry and thermometry of air by use of nonresonant heterodyned laser-induced thermal acoustics," *Applied Optics*, Vol. 40, No. 6, 2001, pp. 965-968.
[33] Hart, R.C., Herring, G.C., and Balla, R.J., "Presure measurement in supersonic air flow by differential absorptive laser-induced thermal acoustics," *Optics Letters*, Vol. 32, No. 12, 2007, pp. 1689-1691.
[34] Jiang, N., Halls, B.R., Stauffer, H.U., Danehy, P.M., Gord, J.R., and Roy, S., "Selective two-photon absorptive resonance femtosecond-laser electronic-excitation tagging velocimetry," *Optics Letters*, Vol. 41, No. 10, 2016, pp. 2225-2228.
[35] Jacobsen, R.T. and Stewart, R.B., "Thermodynamic Properties of Nitrogen Including Liquid and Vapor Phases from 63 K to 2000 K with Pressures to 10,000 Bar," *Journal of Phyiscal Chemistry Reference Data*, Vol. 2, No. 4, 1973, pp. 1-166.